# A *Histoplasma capsulatum* lipid metabolic map identifies antifungal targets and virulence factors

Daniel Zamith-Miranda[1,2,8], Heino M. Heyman[3,8], Meagan C. Burnet[3,8], Sneha P. Couvillion[3], Xueyun Zheng[3], Nathalie Munoz[4], William C. Nelson[3], Jennifer E. Kyle[3], Erika M. Zink[3], Karl K. Weitz[3], Kent J. Bloodsworth[3], Geremy Clair[3], Jeremy D. Zucker[3], Jeremy R. Teuton[3], Samuel H. Payne[5], Young-Mo Kim[3], Morayma Reyes Gil[6], Erin S. Baker[7], Erin L. Bredeweg[4], Joshua D. Nosanchuk[1,2] and Ernesto S. Nakayasu[3,9]*

[1]Department of Microbiology and Immunology, Albert Einstein College of Medicine, Bronx, New York, USA
[2]Division of Infectious Diseases, Department of Medicine, Albert Einstein College of Medicine, Bronx, New York, USA
[3]Biological Sciences Division, Pacific Northwest National Laboratory, Richland, Washington, USA
[4]Environmental and Molecular Sciences Laboratory, Pacific Northwest National Laboratory, Richland, Washington, USA
[5]Department of Biology, Brigham Young University, Provo, UT, USA
[6]Hematology Laboratory, Department of Pathology, Albert Einstein College of Medicine, Bronx, New York, USA
[7]Department of Chemistry, North Carolina State University, Raleigh, North Carolina, USA
[8]These authors contributed equally
[9]Lead contact

*Correspondence: ernesto.nakayasu@pnnl.gov

## SUMMARY

Lipids play a fundamental role in fungal cell biology, being essential cell membrane components and major targets of antifungal drugs. A deeper knowledge of lipid metabolism is key for developing new drugs and a better understanding of fungal pathogenesis. Here we built a comprehensive map of the *Histoplasma capsulatum* lipid metabolic pathway by incorporating proteomic and lipidomic analyses. The map led to the identification of both the fatty acid desaturation and the sphingolipid biosynthesis pathways as targets for drug development. Our analysis also revealed that *H. capsulatum* produces analogs of platelet-activating factor, a potent regulator of the human immune response. Moreover, *H. capsulatum* platelet-activating factor analogs induced platelet aggregation and stimulated the production of the cytokines interleukin-10 and tumor necrosis factor-α by J774 macrophages. Overall, this lipid metabolic map revealed pathways that can be targeted for drug development, in addition to identifying a fungal regulator of the host immune response.

**Keywords**: *Histoplasma capsulatum*, lipid metabolism, drug target, platelet-activating factor, multi-omics analysis

## HIGHLIGHTS

- In-depth characterization of the *Histoplasma capsulatum* lipid metabolism
- Development of a fungal lipid metabolic map based on multi-omics data
- Identification of fatty desaturase and sphingolipid pathways as drug targets
- *H. capsulatum* produces immunoregulatory platelet-activating factor analogs

## INTRODUCTION

Fungal diseases affect more than 1 billion people and cause 1.6 million deaths every year (Bongomin et al., 2017). *Histoplasma capsulatum*, the causative agent of histoplasmosis, is an important pathogen in this context, being associated with HIV infections and a major cause of morbidity and mortality worldwide (Chu et al., 2006). A 2018 Center of Disease Control report reviewed hospitalization data from 2011-2014 in only 12 states in the US and identified 3,409 cases of histoplasmosis with a 7% mortality rate (Armstrong et al., 2018). Serological surveys have shown that sera from 60-90% of individuals are reactive to the *H. capsulatum* antigen histoplasmin in communities surrounding the Mississippi and Ohio basins, suggesting that epidemiological numbers of the disease could be underestimated (Antinori, 2014; Benedict and Mody, 2016). Histoplasmosis treatment relies on only a few antifungal drugs, but the increasing number of resistant strains is a major public health concern (Goughenour and Rappleye, 2017; Parente-Rocha et al., 2017). The absence of immunotherapies and the fact that the newest class of antifungal drugs, echinocandins, which are ineffective against *H. capsulatum*, has already been available for two decades, make the development of new therapies a high priority. A major hurdle in developing new drugs is the limited knowledge about the detailed metabolic reactions and mechanisms of pathogenesis of this microbe.

Lipids have essential roles in many biological processes and the biosynthetic pathways of fungal lipids diverged from metazoan pathways, which makes them obvious antifungal drug targets (Pianalto and Alspaugh, 2016). Indeed, two classes of current antifungal drugs target lipid metabolism: 1) polyenes, including amphotericin B and nystatin, bind and extract ergosterol from the fungal membrane (Anderson et al., 2014; Gray et al., 2012; Palacios et al., 2011); and 2) azoles, such as voriconazole, itraconazole and fluconazole, inhibit cytochrome P-450-dependent 14α-sterol demethylase, an enzyme of the ergosterol biosynthetic pathway (Ghannoum and Rice, 1999; Pianalto and Alspaugh, 2016). More recently, glucosylceramide, a type of sphingolipid that is critical for infection of many fungal species, has been validated as a drug target in *Cryptococcus neoformans* and *Sporothrix* spp. (Artunduaga Bonilla et al., 2021; Mor et al., 2015; Rittershaus et al., 2006).

Lipids have also been characterized as important virulence factors in fungal infections (Hogan et al., 1996). For instance, glycolipids, sterols, as well as the chain length and level of desaturation of fatty acids play a role in pathogenesis (Carratu et al., 1996; Fradin et al., 2015; Nguyen et al., 2011; Nguyen et al., 2009; O'Meara et al., 2018; Rittershaus et al., 2006; Singh et al., 2012). Virulence is not only impacted by specific lipid species, but by how these molecules are organized into larger structures. For instance, ergosterol-dependent microdomains have a crucial role in infectivity (Siafakas et al., 2006; Tagliari et al., 2012). The role of lipids in virulence opens an opportunity to design drugs that target pathogenesis processes rather than the viability of fungal cells (Rella et al., 2016).

There is limited information about *H. capsulatum* lipid composition and function, which is also true for most pathogenic fungi. Polyenes and azoles have been used to treat most mycoses, but many of these fungal species might not even produce ergosterol. Some species produce cholesterol, brassicasterol, lanosterol and other sterols (Weete et al., 2010). In *H. capsulatum*, the levels of phosphatidylcholine correlate with its virulence (Nielsen, 1966). Similarly, perturbations in *H. capsulatum* membrane lipids reduce virulence (Carratu et al., 1996; Maresca and Kobayashi, 1993) and alterations in a delta-9 fatty acid desaturase Ole1 gene enhance temperature sensitivity (Gargano et al., 1995). Also, unsaturated fatty acids decrease in aged yeast cells (Zarnowski et al., 2008). In terms of sphingolipids, *H. capsulatum* also produces glucosylceramides, inositolphosphorylceramides and galactosyl-dimannosyl-inositolphosphorylceramides, which are components of membrane microdomains and are important for infection (Levery et al., 2001; Tagliari et al., 2012; Toledo et al., 2001). We have characterized changes in extracellular vesicle lipid profiles in response to the medium composition (Cleare et al., 2020). In addition, antibodies induce extensive membrane remodeling in *H. capsulatum*, changing its susceptibilty to amphotericin B (Burnet et al., 2020). Considering the importance of lipids, we reasoned that a deeper characterization of *H. capsulatum* lipid metabolism would result in the discovery of virulence factors and drug targets. In this study, we performed an in-depth characterization of the *H. capsulatum* lipid biosynthetic pathway by profiling its lipids and the associated proteins, which were incorporated into a metabolic map. By comparing our results to *Saccharomyces*

*cerevisiae* and humans, we show unique features of the lipid biosynthetic pathway of *H. capsulatum* that can be targeted for drug development. This analysis also led to the discovery that *H. capsulatum* produces analogs of platelet-activating factor (PAF), which we further characterized, including showing that these molecules are biologically active and regulate different aspects of the human immune response.

## RESULTS

### Proteomic and lipidomic analyses and overview of the *H. capsulatum* lipid metabolism

To determine the global landscape of the lipid metabolic pathway of *H. capsulatum*, we performed comprehensive lipidomic and proteomic analyses. Global lipids, including membrane and cytosolic lipids, were extracted using two different methods and submitted to chromatographic separation before analyses by mass spectrometry. Paired global lipidomics and proteomics analyses were performed by submitting the samples to a simultaneous metabolite, protein and lipid extraction (MPLEx) (Nakayasu et al., 2016) (**Figure 1A**). For complementary analyses of sterols, free fatty acids and phospholipids, yeast cells were extracted with two rounds of organic solvent extraction, followed by a solid phase fractionation in a silica 60 column (**Figure 1A**). The extracted fractions were analyzed by either gas chromatography-mass spectrometry (GC-MS) (sterols and fatty acids) or liquid chromatography-tandem mass spectrometry (LC-MS/MS) (sphingolipids, glycerolipids, phospholipids and proteins) (**Figure 1A**).

The combined analysis identified 371 unique lipid species from 5 major lipid categories (fatty acids, sterols, glycerolipids, sphingolipids and glycerophospholipids (phospholipids + lysophospholipids)) that were subdivided into 19 subclasses (**Figure 1B** and **Tables S1-S8**). The most diverse subclasses of lipids in terms of the number of identified species were triacylglycerols (TG), phosphatidylcholines (PC) and phosphatidylethanolamine (PE) with 130, 57 and 51 individual species, respectively (**Figure 1B**). The proteomic analysis led to the identification of 3,215 proteins (**Table S9**). To provide a measurement of the protein abundances in the cells, we calculated the relative copy number of each protein and scaled them into high, moderate, low and very

low abundance (**Figure 1C**), using a scale similar to one previously described (Beck et al., 2011). To validate this scale, we performed a function-enrichment analysis using the KEGG annotation to check the abundance of different pathways. As expected, glycolysis/gluconeogenesis and tricarboxylic acid (TCA) cycle were overrepresented among the highly abundant proteins, whereas DNA replication, nicotinate and nicotinamide metabolism, and basal transcription factors were enriched in moderate, low and very low abundance levels, respectively (**Figure 1D**). The same scale showed that fatty acid metabolism was enriched in highly abundant proteins, whereas steroid biosynthesis proteins were mainly present in moderate abundance (**Figure 1C-D**). Glycerophospholipid and sphingolipid metabolism proteins were not concentrated in a single abundance level and were spread mostly between moderate and low abundant levels (**Figure 1C-D**). The abundance levels of the proteins were directly proportional to each type of lipid in the cellular membrane. For instance, the proteins of fatty acid and steroid (the building blocks of the cell membrane) metabolism were more abundant compared to proteins of the glycerophospholipid, ether lipid or sphingolipid metabolism, which are responsible for the synthesis of lipids from specific lower-abundance classes (**Figure 1D**).

**Lipid biosynthesis and remodeling map of *H. capsulatum***

To provide a global view of *H. capsulatum* lipid metabolism we built a map including lipid biosynthesis and remodeling reactions. The map was constructed based on a metabolic model (Casanovas et al., 2015) structured according to conserved metabolism between *H. capsulatum* vs. *S. cerevisiae*. We added information available for *Cryptococcus neoformans*, one of the best-characterized fungal organisms in terms of lipid metabolism (**Table S10**), along with previous literature on *H. capsulatum*. We used the *H. capsulatum* genomic, proteomic and lipidomic information to further restrict or add reactions that are present in this organism. The *H. capsulatum* map was incorporated with the relative abundance of the lipid species within the same subclass and the protein abundances (**Figure 2).** In terms of fatty acids, species containing 16 and 18 carbons were most abundant. Consistent with figure 1D, 5 out of 10 proteins of this pathway were highly abundant (**Figure 2**). Similarly, 13 of the 23 sterol biosynthesis proteins had

moderate abundance, with ergosterol being the most abundant product (**Figure 2**). In the sphingolipid pathway, ceramides (Cer), hexosylceramide (HexCer), and inositolphosphoceramides (PI_Cer) were the detected lipid species (**Figure 2**). Out of the 9 proteins detected in the proteome, 3 had low abundance, 5 had moderate abundance and 1 was highly abundant (**Figure 2**). The number of low abundant proteins does not necessary mean that the pathway has low activity. For instance, one low abundance protein had more abundant paralogues with the same function (serine palmitoyltransferases Lcb2 vs. Lcb1), and the other two proteins regulate the specific modification of the head group of HexCer, glucosylceramide synthase Gcs1 and endoglycoceramidase-related protein EGCrP1 (**Figure 2**). In terms of glycerolipids, diacylglycerols (DGs) and TGs were identified, being the proteins from this pathway that were present at moderate (2), low (3) and very low abundance (1) (**Figure 2**). Like the free-fatty acid composition, the most abundant species of DGs and TGs had fatty acyl groups with either 16 or 18 carbons attached to them (**Figure 2**). Consistent with the glycerolipids, all the different glycerophospholipid classes had species bearing C16 and C18 as the most abundant in each (**Figure 2**). To increase the utility of the lipid metabolic map, we developed the map into an informatics tool to visualize lipidomics and proteomics data. We tested the tool using lipidomics and proteomics data of *Candida albicans* from a previous publication (Zamith-Miranda et al., 2019), which showed a similar pattern of lipid species with fatty acids containing 16 or 18 carbons in length being the most abundant ones (**Figure S1**).

We further curated the map because homologous genes can have different specificities. We chose to determine the substrates and products of the *H. capsulatum* acyltransferase Ale1 (also known as lysophosphatidylcholine (LPC) acyltransferase 1 – LPT1) because its homolog in *S. cerevisiae* has been shown to modify different classes of lipids (Tamaki et al., 2007). This would allow coverage of a large portion of *H. capsulatum* lipid metabolism. Unfortunately, gene knockout is very difficult in *H. capsulatum* and RNAi experiments often result in a reduction of expression levels that fail to produce a phenotype. Conversely, exogenous expression of genes from the lipid metabolism in biotechnological fungi, such as *S. cerevisiae* and *Yarrowia lipolytica*, has provided important insights on enzyme specificity (Damude et al., 2006; Radovanovic et

al., 2014). Therefore, we performed complementation studies in *S. cerevisiae* with the *H. capsulatum Lpt1* (*Hc-Lpt1*), which would allow curation of a large portion of the metabolic map. A lipidomic analysis was performed in the *Lpt1* knockout strain of *S. cerevisiae* complemented or not with the *Hc-Lpt1* homolog (53% similarity to *S. cerevisiae Lpt1* – *Sc-Lpt1*) (**Figure S2**), using a plasmid with a galactose-inducible promoter. This allows specific expression of *Hc-Lpt1* in the presence of galactose, but not glucose. Both gene knockout and recombinant expression were validated by proteomic analysis (**Figure 3A**). As expected, the Sc-LPT1 specific peptide DISASSPNLGGILK was detected in wild-type *S. cerevisiae*, in both glucose- and galactose-supplemented media (**Figure 3A**). The Hc-LPT1-specific peptide LTAFCWNVHDGR was detected only in complemented strains that were grown in galactose-supplemented medium (**Figure 3A**). The abundance of the peptide KGEELEIVGHNSTPLK from the house keeping protein elongation factor Tu (TUF1) was similar across different samples (**Figure 3A**).

The lipidomics analysis showed that Hc-LPT1 complementation increased the abundances of 60 lipids, including phosphatidic acid (PA), PC, PE, phosphatidylinositol (PI), PS, DG, TG, Cer and mannosyl-inositolphosphoceramide (MIPC) (**Figure 3B-D**, **Table S11**). The Hc-LPT1 complementation also significantly reduced the levels of 77 lipids, including 5 LPC, 3 lysophosphatidylethanolamines (LPE), 2 sphinganines and 3 DG (**Table S12**). On the other hand, disruption of the Sc-LPT1 gene reduced the levels of 30 potential products, including PC, PE, PI, PS and TG. Notably, the proportion of acylated products between the LPT1 from the two species was very different, with PC, PE, PI and PS being more acylated by the *S. cerevisiae* homolog and PA, DG, TG, Cer and MIPC by the *H. capsulatum* counterpart (**Figure 3D**, **Table S13**). The Sc-LPT1 showed a preference for production of lipid species containing short fatty acyl chains, with all the identified products having chains with ≤ 14 carbons (**Figure 3E**). Complementation with *Hc-Lpt1* gene showed a different phenotype, as this homolog produced lipid species containing odd-carbon number (C15 and C17) and longer (≥C18) fatty acyl chains (**Figure 3E**). Overall, the map provides a global view of lipids being produced by *H. capsulatum* along with catalytic enzymes.

**Evolutionary divergent lipid metabolic pathways as drug targets**

We next focused on pathways that could be targeted for antifungal chemotherapies. The ideal drug target is essential for the fungal survival and divergent compared to humans to allow specificity and reduce the chances of side effects. Therefore, we searched the lipid metabolic map for divergent pathways comparing *H. capsulatum* with *S. cerevisiae* and human candidates for anti-*H. capsulatum* drug targets. The most divergent pathways were sphingolipid and fatty acid metabolism (**Figure 4A-B**). In terms of sphingolipids, *H. capsulatum* produces hexosylceramides (glucopyranosylceramides) (Toledo et al., 2001), which are absent in *S. cerevisiae.* Even though both fungi produce inositolphosphoceramides and mannosyl-inositolphosphoceramides, they branch into different products (**Figure 4A**). Whereas *S. cerevisiae* has mannosyl-diinositolphospho-ceramides as a final product, *H. capsulatum* produces galactosyl-dimannosyl-inositolphosphoceramides (Guimaraes et al., 2014) (**Figure 4A**). Also, *H. capsulatum* makes two major pools of ceramide (4-hydroxysphinganine and 9-methyl-4,8-sphingadienine), but *S. cerevisiae* only makes 4-hydroxysphinganine (Toledo et al., 2001). Compared to fungi, humans produce a very distinct profile of sphingolipids. Unlike end products monohexosylceramides of fungi, humans synthesize a much more complex set of glycosphingolipids, including globo, isoglobo, lacto and gangliosides (Merrill, 2011) (**Figure 4A**). Conversely, fungi produce inositolphosphoceramides and their glycosylated derivates, which are absent in humans. Humans also produce sphingomyelins, which are absent in fungi (**Figure 4A**). The sphingolipid pathway can, therefore, be an excellent drug target due to these major differences in composition compared to humans.

In fatty acid metabolism, humans are unable to perform the first two steps of fatty acid desaturation and instead uptake the respective unsaturated fatty acids from food, while *S. cerevisiae* has only one fatty acid desaturase gene (delta-9 desaturase, also known as oleate synthase *Ole1*) in its genome (**Figure 4B**). In addition to Ole1, *H. capsulatum* has a gene annotated as delta-12 desaturase (*FAD2*) and two uncharacterized desaturases (HCBG_08514 and HCBG_05092), which collectively might be responsible for the production of fatty acids with 2 and 3 double bonds (**Figure 4B**). We examined the distribution of fatty acyl chains that are incorporated into *H. capsulatum*

and *S. cerevisiae* lipids. The results showed that both fungi incorporate fatty acyl groups with different chain lengths into their lipids. *S. cerevisiae* incorporates significantly more fatty acyl chains with less than 16 carbons (by Fisher's exact test), whereas *H. capsulatum* has significantly more lipids with fatty acids longer than 17 carbons (**Figure 4C**). In terms of unsaturation, *S. cerevisiae* had almost exclusively saturated lipids or fatty acyl chains with 1 double bound, whereas *H. capsulatum* had fatty acyl chains with 2 or 3 double bonds (**Figure 4D**). To develop further insights on the enzymes responsible for desaturating these fatty acids, we expressed all 4 *H. capsulatum* desaturase candidates in *S. cerevisiae* by galactose induction, and determined the fatty acid composition by methylating them and analyzing by them GC-MS. We also included *S. cerevisiae* Ole1 as a positive control for over-expression. *S. cerevisiae* Ole1 over-expression increased the ratios of C14:1/C14:0, C16:1/C16:0 and C18:1/C18:0 by 4.0, 3.0 and 9.4 fold, respectively (**Figure S3A**), whereas the *H. capsulatum* Ole1 increased the ratios of C14:1/C14:0, C16:1/C16:0 and C18:1/C18:0 by 11%, 24% and 81%, respectively (**Figure S3A**). The expression of HCBG_08514 and HCBG_05092 had almost no impact on the saturation levels of the fatty acids (**Figure S3A**), which could be due to the lack of the precursors in *S. cerevisiae*. C16:2 (9Z,12Z-hexadecadienoic acid), C18:2 (9Z,12Z – linoleic acid) and C18:3 (9Z,12Z,15Z – α-linolenic acid) were only detected when *H. capsulatum* FAD2 was expressed (**Figure S3A-B**). A composition analysis of *H. capsulatum* fatty acids revealed two low abundance peaks of C18:3, one being α-linolenic acid and a second peak that did not match to any available standard (**Figures 4E-F and S3C**). These results showed that *H. capsulatum* FAD2 is indeed a bifunctional delta-12/delta-15 desaturase, which helps further curate the lipid metabolic map (**Figure 2**, top left). Similar to sphingolipids, the *H. capsulatum* fatty acid desaturase pathway represents a potential target.

To perform a proof-of-concept that sphingolipid and fatty acid desaturation pathways can be targeted for drug development, we tested the effects of myriocin (serine-palmitoyltransferase inhibitor, which blocks the first step of sphingolipid biosynthesis pathway), and 10-thiastearic acid and thiocarlide (two fatty acid desaturase inhibitors) on *H. capsulatum* growth. Myriocin, 10-thiastearic acid and thiocarlide showed minimum-inhibitory concentrations (MICs) of 0.03, 1.25 and 12.5 μM, respectively (**Figure 5A**). To confirm that these compounds target fatty acid desaturases and sphingolipid

biosynthesis, we performed a fatty acid analysis on treated and unexposed yeast cells. Cells were grown for 48 hours with one half of the MIC and fatty acids were extracted, methylated and analyzed by GC-MS. 10-Thiastearic acid did not affect the ratio between unsaturated and saturated fatty acids (**Figure 5B**), suggesting that this compound might target other pathways rather than the fatty acid desaturation. As expected, thiocarlide reduced the C18:2/C18:0 peak area ratio from 11.4 to 8.5 (25% reduction), the C18:1/C18:0 ratio from 4.5 to 3.7 (18% reduction) and the C20:1/C20:0 ratio from 1.3 to 0.8 (39% reduction) (**Figure 5B**). Conversely, the C16:1/C16:0 ratio had a slight increase from 0.036 to 0.044 (22% increase) (**Figure 5B**). We also performed a lipidomic analysis on cells grown with or without one half of myriocin MIC for 48 hours. As expected, the most abundant ceramide species, Cer(d18:1/24:0(2OH)) and Cer(d20:0/24:0), were reduced by 52% and 62%, respectively (**Figure 5C**). As a control of a lipid from an unrelated class, the level of the most abundant DG, DG(16:0/18:2/0:0), increased by 51% (**Figure 5C**). To further test the fatty acid desaturation and sphingolipid pathway as anti-*H. capsulatum* drug targets, we tested the ability of these inhibitors to reduce intracellular infection by treating infected alveolar macrophages with 2x MIC of each compound. We chose alveolar macrophages as they are the primary cells targeted by *H. capsulatum* in infection (Deepe and Buesing, 2012). Thiocarlide reduced the intracellular *H. capsulatum* load by approximately 30%, whereas 10-thiastearate and myriocin had no significant effect (**Figure 5C**). These results showed that thiocarlide reduces intracellular infection with *H. capsulatum*, while modification of 10-thiastearate and myriocin might need structural modifications or different delivery strategies to become more effective in killing intracellular fungi. These results validate the fatty acid desaturation and sphingolipid pathways as a potential target for developing anti-*H. capsulatum* drugs, and that thiocarlide can reduce intracellular fungal load in alveolar macrophages.

**Discovery and validation of platelet-activating factor analogs in *H. capsulatum***

One notable unique lipid found in the *H. capsulatum* lipidomics analysis was PC(16:2/2:0) (**Figure 6A**). This lipid is analogous to the canonical platelet-activating factor (PAF), a PC species containing ether-linked C16:0 chain in the *sn1* position and acetyl group in the *sn2* position (2-O-acetyl-1-O-hexadecyl-sn-glycero-3-phosphocholine –

PC(O-16:0/2:0)) (**Figure 6B**). PAF is a major regulator of the immune response in mammals (Prescott et al., 2000). Therefore, we sought to further validate the structure of the *H. capsulatum* PAF analog. We searched for other lipids containing acetate as a fatty acyl chain in our lipidomics data and found another species, PC(16:1/2:0) (**Figure S4**). In *S. cerevisiae*, ester-linked PAF (acyl-PAF) analogs are produced by LPT1 (Nakayama et al., 1994; Tamaki et al., 2007). We observed that Sc-LPT1 knockout strain had drastically reduced amounts of PC(16:1/2:0) (**Figure 6C**). Unfortunately, the *H. capsulatum* preferred substrate LPC(16:2/0:0) is not present in *S. cerevisiae*, due to the absence of additional desaturases in this species. Nevertheless, complementation of the *S. cerevisiae* LPT1-knockout strain with the Hc-LPT1 homolog increased the abundance of PC(16:1/2:0) (**Figure 6C**), showing that LTP1 is a candidate for PAF-analog synthase in *H. capsulatum*.

We next aimed to compare our molecule to a chemically synthesized standard, but unfortunately, PC(16:2/2:0) and PC(16:1/2:0) standards were not commercially available. The lack of knowledge on the double bond position prevented the synthesis of the lipid with the right fatty acyl group. We reasoned that *H. capsulatum* could be producing a saturated version of these lipid species (1-palmitoyl-2-acetyl-sn-glycerol-phosphocholine – PC(16:0/2:0 – acyl-PAF) – which is commercially available) (**Figure 6B**), although in smaller amounts. The liquid chromatography-tandem mass spectrometry analysis found a peak with the expected *m/z* (mass-to-charge ratio) and retention time (**Figure 6D**). To ensure that the sample background would not cause retention time shift, the sample was spiked with the standard and analyzed in parallel, which showed a consistent elution pattern with the standard alone and the endogenous species (**Figure 6D**). Tandem mass fragmentation of this species showed a major fragment at *m/z* 184.07, derived from the breakage of the phosphocholine (ChoP) head group (**Figure 6E**). Because tandem mass fragmentation of lipid species often generates only a few fragments, which is not optimal to confidently identify a molecule, we performed ion-mobility spectrometry coupled with mass spectrometry (IMS-MS) analysis. In the drift tube where the IMS-MS analyses were performed, the ions were gently pulled by a weak electric field through the nitrogen gas-filled tube. As the ions collided with the gas molecules, they were separated based on their shape and size, allowing the separation of isobaric molecules which cannot be

distinguished by *m/z* alone. The *H. capsulatum* lipid extract was fractionated using a C18 column coupled to an HPLC system and fractions enriched with the lipids of interest were collected and analyzed by IMS-MS. The results showed a consistent drift time and collision cross section values when comparing the endogenous PC(16:0/2:0) to the synthetic standard (**Figure 6F**). Overall, the retention time, high mass accuracy, tandem mass fragmentation and drift time of the IMS-MS analyses consistently support the presence of ester-linked acetylated PCs in *H. capsulatum*.

### *H. capsulatum* PAF analogs are biologically active

To determine if the *H. capsulatum* PAF analogs have similar activity compared to the human canonical PAF, yeast lipid extracts containing *H. capsulatum* PAF analogs (fractions 8-10 from HPLC separation) were tested for their ability to aggregate platelets. Platelet aggregation was measured by electrical impedance in human whole blood. This technique measures the increase in electrical resistance (measured in OHMS) between two electrodes caused by the deposition of aggregating platelets (Femia et al., 2013). The addition of the *H. capsulatum* fractions containing PAF analogs led to a rapid induction of platelet aggregation, like the positive controls with the canonical PAF, PC(16:0/2:0) (acyl-PAF) and arachidonic acid (**Figure 7A-B**).

We also tested the HPLC fractions enriched in *H. capsulatum* PAF analogs in their ability to induce cytokine production in J774 macrophage-like cells. As measured by ELISA, the fractions induced a dose-dependent production of interleukin-10 (IL-10) and tumor necrosis factor (TNF)-α in pico to nanomolar range (estimated based on peak area relative to external standards), which is consistent with the activity of the PC(16:0/2:0) standard (**Figure 7C-D**). The highest tested concentration of the lipid fractions and standard induced the production of a smaller amount of TNF-α (**Figure 7C-D**), probably due to receptor saturation or negative feedback mechanisms. The production of TNF-α and IL-10 were inhibited by the PAF receptor antagonist WEB2086 (**Figure 7C-D**), showing that *H. capsulatum* PAF analogs regulate J774 cells by engaging the PAF receptor.

Taken together our data show that *H. capsulatum* produces bioactive PAF analogs that activate platelets and induce cytokine production in host effector cells.

## DISCUSSION

Here we developed a global map of the *H. capsulatum* lipid metabolism by incorporating genomic, proteomic and lipidomic information, including relative abundances of proteins and lipids. We found accordance of the protein abundance levels with their functions in the lipid metabolism. For instance, the proteins involved in the synthesis of the major lipid components--the fatty acids and sterols--were enriched among the high and moderate abundant proteins, whereas the proteins related to the synthesis of specific lipid head groups were enriched in the low to very low abundant proteins. This might be a consequence of cell resource optimization as protein synthesis is one of the most energetically expensive tasks in cells (Metzl-Raz et al., 2017). Our lipid map also showed that TG, PC and PE are the most diverse classes of lipids, which is in agreement with the fact that they are most abundant ones (Domer and Hamilton, 1971). Our results show that the diversity of TG, PC and PE species could be due to fatty acid remodeling, as these lipids are products of the LPT1 acyltransferase. LPT1 transfers acyl groups to a variety of fatty acyl chains, including odd-carbon chains (C15 and C17) and long-chain (≥C18) fatty acids. Our experiments with LPT1 also helped to curate the lipid map since the *S. cerevisiae* homolog has a different specificity for substrates, that being a major impact in producing phospholipids with short fatty acyl chains. In *S. cerevisiae*, the substrates of LPT1 have been shown *in vitro*, using radioactive precursors to acylated LPC, LPG, LPA, LPE, LPI and LPS (Tamaki et al., 2007). The acylation of LPA, a central precursor for all glycerolipids and glycerophospholipids, suggests that the LPT1 impact could be indirect. Therefore, further investigation will be needed to determine if this enzyme can directly acylate DG into TG. We also curated the fatty acid desaturation pathway by expressing *H. capsulatum* desaturase candidate genes in *S. cerevisiae*. We validated that Ole1 has delta-9 desaturase activity. In addition, we show that FAD2 is indeed a bifunctional delta-12/delta-15 desaturase. In fungi, delta-15 and bifunctional delta-12/delta-15 desaturases evolved from delta-12 desaturases in multiple independent gene duplications, which complicates the assignment of their specificity based on their sequence (Damude et al., 2006). This scenario is a little different in *H. capsulatum*, as *H. capsulatum* FAD2 evolved to have both activities within a single gene copy rather than duplicating the gene.

We identified the fatty acid desaturation and the sphingolipid pathways as divergent points in the lipid metabolism pathways of *H. capsulatum* vs. *S. cerevisiae* and humans. We showed that these two pathways are potential targets for developing anti-histoplasmosis drugs. Thiocarlide (also known as isoxyl) is a potent inhibitor (nanomolar range) of *Mycobacterium tuberculosis* delta-9 stearoyl desaturase and was used as a second line of anti-tuberculosis drugs in the 1960s (Phetsuksiri et al., 1999; Phetsuksiri et al., 2003). However, despite its low toxicity, thiocarlide was not as effective during clinical trials, so is no longer used to treat patients (Phetsuksiri et al., 1999; Tousek, 1970; Urbancik, 1970). One possible explanation for the clinical trial failure is the poor solubility of the compound in water. Since then, other drug delivery vehicles have been tested with promising results *in vitro* (Wang and Hickey, 2010). Delta-12 oleate desaturase has been validated as a drug target in the protozoan parasite, *Trypanosoma cruzi* (Maldonado et al., 2006). Indeed, thiocarlide inhibited *T. cruzi* growth in low micromolar range and reduced the levels of unsaturated fatty acids by approximately 30% (at 10 μM concentration) (Alloatti et al., 2009). These numbers are similar to the MIC and reduction in unsaturated fatty acid level for *H. capsulatum* (**Figure 5A-B**). The small changes in unsaturated fatty acid levels were associated with a drastic reduction in cell viability, which suggests that homeostasis in membrane fluidity is crucial for life. In addition, thiocarlide induced a reduction in intracellular infection of alveolar macrophages, further supporting its potential as therapeutic target. Our data also showed that 10-thiastearic acid might target a different pathway rather than fatty acid desaturation. This is expected to some extent since 10-thiastearic acid is a fatty acid analog; therefore, it is more likely to inhibit other processes of fatty acid metabolism. However, this type of molecule should still be considered as a drug candidate due to its antifungal activity and possible low toxicity to humans. The 10-thiastearic acid analog tetradecylthioacetic acid has a low toxicity in humans up to 1 g/day (Pettersen et al., 2008). Unlike thiocarlide, 10-thiastearic acid and myriocin were unable to reduce the intracellular *H. capsulatum* load in macrophages. However, this fungus is a facultative intracellular pathogen and the drug could be effective in killing extracellular yeasts. In addition, engineered delivery methods, such as liposomes, and structural modifications, such as esterification, can further improve the bioactive compound to reach the intracellular milieu. Therefore, 10-

thiastearate and myriocin might still be useful for treating histoplasmosis but further development still needs to be performed to test their efficacy.

We also performed a proof-of-concept that sphingolipids are promising targets for anti-histoplasma drug development by inhibiting the first step of the sphingolipid pathway with myriocin. Myriocin kills *Candida albicans* and *Aspergillus fumigatus* in micromolar concentrations (Kluepfel et al., 1972; Perdoni et al., 2015). *H. capsulatum* is more sensitive to myriocin as its MIC was 30 nM (**Figure 5B**). Unfortunately, myriocin has immunosuppressant activity (de Melo et al., 2013; Strader et al., 2011), but this has been explored for simultaneously killing the fungus and reducing the pathogenic inflammation of the lungs in cystic fibrosis mice infected with *A. fumigatus* (Caretti et al., 2016). The fact the *de novo* sphingolipid synthesis is essential for *H. capsulatum* opens the opportunity to explore other inhibitors of serine palmitoyltransferase, or other enzymes in the pathway. Indeed, other enzymes of the fungal sphingolipid pathway have been validated as drug targets. In *C. neoformans*, acylhydrazones have been shown to be potent inhibitors of the glucosylceramide synthesis (nanomolar range) and excellent antifungal drug candidates (Lazzarini et al., 2018; Mor et al., 2015). Sphingolipids have also been shown to be a mechanism of azole-resistance in *C. albicans* (Gao et al., 2018) and at the same time, excellent targets for synergistic drugs across multiple species (Spitzer et al., 2011).

Our study also led to the identification of PAF analogs in *H. capsulatum*. Such analogs were previously described in *S. cerevisiae*, which is synthesized by the acyltransferase LPT1 (Nakayama et al., 1994; Tamaki et al., 2007). Complementation of the *S. cerevisiae* LPT1-knockout strain with the Hc-LPT1 homolog significantly increased the abundance of PC(16:1/2:0), but not at the same extent of the WT *S. cerevisiae* strain. LPT1 may be PAF synthase in *H. capsulatum*. However, this and other possibilities, such as PAF being synthesized by a different acyltransferase, need to be confirmed with more experiments. The *H. capsulatum* PAF analogs showed biological activity by inducing platelet aggregation in human blood. The analogs also activated macrophages, as seen by the production of cytokines, an event that was PAF receptor dependent. Although PAF analogs *per se* were able to induce the production of cytokines by macrophages, it is possible that in a complex scenario, as *in vivo*, the analogs could modulate the production

of other cytokines, when in the presence of live yeast in the host. PAF is a water-soluble lipid that has a variety of functions in regulating the host immune response and it is essential for neutrophil recruitment to the site of infection in histoplasmosis (Medeiros et al., 2015). Besides being water soluble, it is also possible that the *H. capsulatum* PAF analogs are being delivered to the host via extracellular vesicles secreted by this fungus (Albuquerque et al., 2008; Cleare et al., 2020). Endogenous acyl-PAF from mice has some PAF receptor agonistic effects in lower concentrations, but can become antagonists depending on the concentration and physiological condition (Chaithra et al., 2018). Therefore, *H. capsulatum* PAF analogs may play a role in controlling the immune response against histoplasmosis, making the host environment more permissive to fungal survival.

In conclusion, we built a detailed map of *H. capsulatum* lipid metabolism based on omics data. Our data identified defined regions of the *H. capsulatum* lipid metabolic pathway that can be targeted for drug development and our analyses led to the characterization of interesting lipid species that have immunoregulatory activities.

**Limitations of study**

One limitation of this study is that *H. capsulatum* is a fungus with few genetic engineering tools, which makes the execution of gene knockout or knockdown experiments highly challenging. Therefore, we utilized the gene complementation system in *S. cerevisiae* to study the specificity of genes from the lipid metabolism. We found dozens of *H. capsulatum* LPT1 products and determined the double bond positions catalyzed by FAD2, but the complementation system can generate false negatives due to the absence of specific substrates in *S. cerevisiae*. The different lifestyles between *H. capsulatum* and *S. cerevisiae* limits some of the comparisons between the lipid composition of these two organisms. Another limitation of our study is that the *H. capsulatum* lipidomic analysis was performed in a single growth condition, which might not fully recapitulate the *in vivo* environment during infection. Also, we have previously shown that different growth conditions have an impact on the composition of extracellular vesicles, including variations in lipid profiles (Cleare et al., 2020). Therefore, the analysis of different growth

conditions and forms of the fungus might lead to different lipid profiles and even the identification of additional lipid species.

## Material and Methods

### Cells

*Histoplasma capsulatum* G217B strain and murine alveolar macrophages AMJ2 was purchased from the American Type and Culture Collection (ATCC, Manassas, VA). *S. cerevisiae* deficient LPT1 gene (YOR175C knockout (KanMX), strain 12431) and wild-type strains (BY4742; mat alpha, his3Δ1 leu2Δ0 lys2Δ0 ura3Δ0) were purchased from Dharmacon (Lafayette, CO).

### *Saccharomyces cerevisiae* transformation

Strains were maintained on YPD (2% glucose, 10 g/L peptone, 10 g/L yeast extract) or YNB with amino acid supplements (2% glucose, 1.7 g/L YNB salts without ammonium sulfate or amino acids (Difco), 5 g/L ammonium sulfate (Fisher), +/- 50 mg/L leucine, lysine, histidine (LLH) and uracil). The strains were transformed by a lithium-acetate-heat shock method (Gietz et al., 1995) with a plasmid containing the *H. capsulatum* acyltransferase LPT1 (Uniprot ID C0NZS2), or desaturases Ole1 (Uniprot ID C0NLE5), FAD2 (Uniprot ID C0NKL1), HCBG_08514 (Uniprot ID C0NZD4) and HCBG_05092 (Uniprot ID C0NPL2) genes and *S. cerevisiae* Ole1 (Uniprot ID P21147) that were codon optimized, synthesized and cloned into the Gal-inducible plasmid pESC-URA by GenScript (Piscataway, NJ). Briefly, 500 µL of cells grown in YPD for 16 h were spun down, and the supernatant removed. Added to the BY4742 and #12431 cells were: 5 µg of herring sperm DNA (5 µL of 10 mg/mL stock), and 400 ng of GenScript plasmid DNA, 500 µL of PLATE buffer (40% PEG 3350, 0.1 M lithium acetate, 10 mM Tris HCl (pH 8.0), 1 mM EDTA), and 57 µL DMSO. Cells were incubated at room temperature for 15 min, followed by 15 min at 42 ºC. Cells were collected by brief centrifugation of 5 s at 8000 x g, supernatant removed, resuspended in PBS, then plated on YNB-2% glucose-LLH 2 % agar plates without uracil. Resulting colonies were screened for plasmid presence by PCR of a portion of the pESC-URA-lpt1 plasmid (Forward primer: 5'-TTGGAAACAGCTCCAAATCC-3', Reverse primer: 5' CCCAAAACCTTCTCAAGCAA-3'; ordered from ThermoFisher Oligos) and preserved as glycerol stocks.

### *S. cerevisiae* plasmid expression assays

For the Hc_LPT1 and desaturase expression assays, cells were pre-cultured overnight in YNB 2% glucose LLH +/- uracil to accommodate the non-plasmid strain auxotrophy as a negative control. For biomass collection during induction, which often slows or prevents cell division, cells were inoculated to an OD of 0.5 into YNB-2% galactose LLH +/- uracil, and collected after induction of plasmid expression for 17 hours. LPT1 cultures were also analyzed after 17 hours grown in glucose LLH +/- uracil (uninduced). Cultures were collected by spinning 25 mL of culture in a tabletop centrifuge (VWR symphony 4417 R) at 2000 x g for 2 min with a swinging bucket rotor fitting 50-mL conical tubes. Pellets were collected into pre-weighted tubes and washed 2X with TBS before flash freezing in liquid nitrogen. All samples were done in 4 replicates as input for downstream omics analysis.

### ***Histoplasma capsulatum*** **cell culture**

*H. capsulatum* G217B was grown in yeast form at 37°C in Ham's F12 medium as previously described (Matos Baltazar et al., 2016). Cells were harvested by centrifuging at 2000 x *g* for 2 min and washed twice with PBS. All the sample preparation and analysis were done in 4 replicates and in a randomized order to ensure the biological significance and prevent batch effects.

### **Sample extraction and fractionation on Silica 60 column**

Samples were extracted using two different approaches. For global proteomics and lipidomics analyses, samples were submitted to Metabolite, Protein and Lipid Extraction (MPLEx) as previously described (Nakayasu et al., 2016). For the fractionation study, cells were suspended in 400 µL of water and transferred to PTFE-lined 13x100-mm Pyrex glass tubes (prewashed with chloroform:methanol (2:1, v:v) and chloroform:methanol:water (1:2:0.8, v:v:v)) containing 200 µL of silica/zirconia beads (Vallejo et al., 2012). 1 mL of methanol and 0.5 mL of chloroform to form chloroform:methanol:water (1:2:0.8, v:v:v) solution and extracted by vortexing for 2 minutes followed by centrifugation for 10 minutes at 1,800 x *g* at room temperature. The supernatants were collected into clean glass tubes. Samples were additionally extracted twice with 1 mL of chloroform:methanol (2:1, v:v) and once with 1 mL of

chloroform:methanol:water (1:2:0,8, v:v:v), and the supernatants were pooled together then dried in a vacuum centrifuge. Extracted lipids were fractionated into neutral lipids, fatty acids and phospholipid fractions using Silica 60 columns (Albuquerque et al., 2008) and dried in a vacuum centrifuge.

**High performance liquid chromatography (HPLC) fractionation of phospholipids**

The phospholipid fraction from the Silica 60 separation was reconstituted in 2 mL methanol:dichloromethane (8:2), centrifuged and the supernatant was loaded (100 µL) onto a reverse-phase column (Kinetex®, Torrance, CA, 150 x 4.6 mm, 2.6 µm, C18, 100 Å,) coupled to a 1200 Agilent HPLC and fraction collector (Agilent™, Santa Clara, CA, USA). The samples were loaded in the column equilibrated with 60% solvent A (60:40 acetonitrile:water + 10 mM ammonium acetate) in 40% solvent B (90:10 isopropanol:acetonitrile + 10 mM ammonium acetate) and the elution was performed at a flow rate of 0.5 mL/min using the following gradient: 40-50%B in 2 min, 50-60% B in 1 min, 60-70% B in 9 min, hold in 70% B for 3 min, 70-78% B in 2 min, 78-85% B in 2 min, 85-99%B in 6 min and hold at 99% B for 3 min. Eluting lipids were monitored by electrospray ionization mass spectrometry (LTQ™ Linear Ion Trap Mass Spectrometer, Thermo Scientific™, Waltham, MA, USA) with 26 fractions collected in regular intervals of 1 min from RT 2.5 min – 28.5 min. Fractions from 18 fractionation runs were dried in a vacuum centrifuge and dissolved in an appropriate solvent for subsequent analyses.

**Proteomic analysis**

Extracted proteins were suspended in 100 µL of 8 M urea in 50 mM $NH_4HCO_3$ and protein concentration was determined by a BCA protein assay (Thermo Scientific, Rockford, IL). Samples were digested as previously described (Matos Baltazar et al., 2016) and desalted using 1 mL Discovery C18 SPE columns (Supelco, Bellefonte, PA). Digested peptides were suspended in water, quantified by BCA assay and had their concentrations adjusted to 0.1 µg/µL with water. A total of 500 ng of peptides were direct injected onto the analytical column. The analytical column used was prepared in-house by slurry packing 3-µm Jupiter C18 stationary phase (Phenomenex, Torrence, CA) into a 70-cm long, 360 µm OD x 75 µm ID fused silica capillary tubing (Polymicro Technologies

Inc., Phoenix, AZ). The column was coupled to a Waters M-ClassTM UPLC system (Millford, MA) connected with a Q-Exactive Plus hybrid quadrupole/Orbitrap mass spectrometer from Thermo Fisher Scientific (San Jose, CA). Mobile phases consisted of 0.1% formic acid in water (MP-A) and 0.1% formic acid in acetonitrile (MP-B). The gradient elution, and column regeneration profile was as follows (min:%MP-B); 0:0.1, 4.0:8, 36:12, 135:30, 175:45, 180:95, 190:95, 195:1. Data acquisition (180 min) was started at the end of the sample loading period (20 min). The analytical column was coupled to the Q-Exactive using a home-built nanospray adapter interface with 2.2 kV applied to achieve electrospray ionization. The MS inlet was maintained at a temperature of 275 °C. A precursor scan was performed from *m/z* 400 to 2000 at a resolution of 35k at *m/z* 400 and automatic gain control (AGC) of 3e6. Operated in data-dependent mode, the top 12 most intense ions from the precursor scan were selected for high energy collision dissociation (HCD) MS/MS at a resolution of 17.5k, AGC of 1e5, isolation window of 2 m/z, and a max ion time of 100 ms. Only ions identified as having a +2 charge or higher were subjected to HCD and subsequently excluded from further analysis for 30 sec thereby allowing for deeper coverage.

LC-MS/MS data were analyzed with MaxQuant software (v.1.5.5.1) by searching against the *H. capsulatum* G186AR (downloaded August 15, 2016) and *S. cerevisiae* S288c (downloaded January 11, 2018) sequences from Uniprot Knowlegdgebase, considering protein N-terminal acetylation and oxidation of methionine as variable modifications, and cysteine carbamidomethylation as a fixed modification. The parent ion mass tolerance was set at 20 and 4.5 ppm for the first and main peptide searches, whereas the fragment mass tolerance was set as 20 ppm for both searching rounds. Tryptic digestion was required for peptide termini and up to 2 missed cleavage sites were allowed per peptide.

Protein abundances were estimated by the intensity-based absolute quantification (iBAQ) method (Wilhelm et al., 2014). The intensities were normalized by the total iBAQ sum of each sample and expressed as relative number of protein copies (percentage from total). Proteins were classified according to their abundance converting number of copies described by Beck et al. (Beck et al., 2011) to the relative number of protein copies (%).

Function-enrichment analysis was performed as described previously (Baltazar et al., 2018).

**Lipid analysis by liquid chromatography-tandem mass spectrometry**

Total lipid extracts and phospholipid fraction from the Silica 60 column were resuspended in methanol and subjected to LC-MS/MS analysis as previously described (Dautel et al., 2017). To assess the technical variability, we spiked in the SPLASH Lipidomix standard (Avanti Polar), which contains a mix isotopically labeled lipids. Lipid species were identified using LIQUID and manually inspected for validation. The features of the identified lipid species were extracted and aligned using MZmine (Pluskal et al., 2010). For comparative purposes, lipids were considered significantly different with $p \leq 0.05$ by *t*-test considering equal variance and unpaired samples. The distribution of fatty acyl groups was done by counting individual fatty acyl groups and were considered significantly different with a $p \leq 0.05$ by Fisher's exact test.

**Lipid Analysis by ion mobility spectrometry-mass spectrometry (IMS-MS)**

HPLC-fractionated fractions were suspended in methanol and analyzed on an Agilent 6560 IMS-QTOF MS platform (Agilent Technologies, Santa Clara, CA) (Zhang et al., 2016). For IMS measurements, ions were generated by an electrospray ionization source, passed through the glass capillary, focused and accumulated in the ion funnel before being pulsed into the IMS drift tube filled with ~ 3.95 torr of nitrogen gas, where they traveled under the influence of a weak electric field (10-20 V/cm). Ions exiting the drift tube are then refocused by a rear ion funnel prior to being detected by QTOF MS, and their arrival times were recorded. Collision-cross section (CCS) which contains information of molecule size and shape can be determined from the data acquired under different electric fields. The Agilent IM-MS Browser software was used to process IMS data, extract IMS profiles and calculate CCS values. Candidate phospholipid species were matched to standards based on their CCS values and MS/MS spectra.

**Fatty acid and sterol analyses**

Fatty acid fractions from the silica 60 column fractionation were resuspended in 0.5 mL of anhydrous methanolic HCl (1.2 N), sealed and incubated for 1 h at 100°C. After cooling, 0.5 mL of water was added and the fatty acid methyl esters (FAMEs) were extracted by adding 0.5 mL hexane and vortexing the samples. Sterol fractions were treated with 30 mg/mL methoxyamine in pyridine for 90 min at 37 °C with shaking, and were derivatized with N-methyl-N-(trimethylsilyl)trifluoroacetamide (MSTFA) (Sigma-Aldrich) with 1% trimethylchlorosilane (TMCS) (Sigma-Aldrich) at 37°C with shaking for 30 min (Kim et al., 2013). Derivatized FAMEs and sterols were then analyzed by GC-MS. For the background referencing and retention time calibration, blanks and FAME standard mix (C8-28) (Sigma-Aldrich) were also analyzed. Analyses were performed in an Agilent GC 7890A using an HP-5MS column (30 m × 0.25 mm × 0.25 µm; Agilent Technologies, Santa Clara, CA) coupled with a single quadrupole MSD 5975C (Agilent Technologies). For each analysis 1 µL of sample was injected (splitless) into the injection port with constant temperature at 250°C. The GC analysis started with an initial oven temperature fixed at 60°C for 1 minute after injection, and then the temperature was increased to 325°C at a rate of 10°C/minute, and finished with a 5-minute hold at 325°C. The data files were calibrated and deconvoluted with Metabolite Detector as stated previously (Hiller et al., 2009). Molecules were identified by library matching against the FiehnLib (Kind et al., 2009) with some in-house added entries. Unidentified chromatographic features were also searched against the Wiley Fatty Acids Methyl Esters Mass Spectral Database and the NIST17 GC-MS spectral library.

**Evaluation of lipid biosynthesis inhibitors on *H. capsulatum* axenic and intracellular growth**

The tested compounds (myriocin, 10-thiastearic acid and thiocarlide) were serially diluted in round bottom 96-well plates. *H. capsulatum* yeast cells were washed with PBS and suspended in Ham's F12. Yeast cells were added in 4 replicates to the drug-containing plates at a final cellular density of 2.5 x $10^4$ cells/mL. The plates were incubated at 37 ºC under constant shaking for 7 days until the optical analysis of growth. The drug concentration present in the set of replicates with no visual growth was considered the MIC for each of the drugs. To evaluate the effect of lipid synthesis inhibition of *H.*

*capsulatum*, $10^6$ cells/mL were incubated in Ham's F12 in the presence or absence of myriocin, 10-thiasteric acid and thiocarlide in half of the evaluated MIC for each drug. The cultures were kept at 37 ºC shaking at 250 rpm for 48 h. Cells were extensively washed with ice-cold PBS and pellets were frozen for further lipid extraction and subsequent fatty acid and lipidomics analyses. This experiment was performed in triplicates. Murine alveolar macrophage cell line AMJ2 was plated onto 96-well plates and incubated overnight at 37 ºC with 5% $CO_2$. The macrophages were challenged with *H. capsulatum* (ratio of 2 yeasts per macrophage cell) in the presence or absence of myriocin, 10-thiasteric acid and thiocarlide at 2x their MIC for 48 hours. Macrophages were lysed with distilled water and the yeast suspensions were diluted and plated onto BHI-agar supplemented with 5% of sheep's blood. Plates were incubated at 37 ºC and colony forming units were counted after grown.

**Platelet aggregation assay**

Platelet aggregation was measured in a Chrono-Log 700 aggregometer by impedance in whole blood. Electrical impedance shifts that correspond to platelet aggregation were captured in real-time with the addition of *H. capsulatum*-derived fractions. Controls included arachidonic acid, acyl-PAF [PC(16:0/2:0)] or PAF [(PC(O-16:0/2:0)].

**Treatment of macrophages with *H. capsulatum* lipid fractions**

J774 macrophage-like cell line was cultivated in DMEM medium containing 10% FBS at 37°C and 5% $CO_2$ atmosphere. Cells were treated for 24 h with lipids fractionated by HPLC. Due to the lack of the exact concentration of the lipid fractions, these were tested in 4 dilutions: $10^{-3}$, $10^{-4}$, $10^{-5,}$ and $10^{-6}$. Controls and treatments were carried in the presence or absence of the PAF receptor antagonist WEB 2086, and vehicle only (same amount as in the highest concentration of the fractions – 0.1%). After treatment TNF-α and IL-10 were measured by ELISA (B&D). Results were analyzed with GraphPad (Prism) and were considered significant with $p \leq 0.05$ by ANOVA followed by Tukey's multiple comparison test.

### Construction of the *H. capsulatum* lipid metabolic map

We have built a preliminary G217B lipid map with a tool name VANTED v2.6.5 (Hartmann and Jozefowicz, 2018), using the *S. cerevisiae* model (Casanovas et al., 2015) as a starting point. Enzyme homologs were identified by blasting *S. cerevisiae* and *C. neoformans*, two of the best-characterized fungi in terms of lipid metabolism (Casanovas et al., 2015; Munshi et al., 2018). We also based the map on the information available on the *H. capsulatum* from the lipid literature and lipids identified in the lipidomics analysis. The map was integrated by adding the abundance level of lipids using their relative mass spectrometry intensities within the same lipid class.

### Lipidomics and proteomics visualization tool

We developed a software tool based on the lipid metabolic map to automatically build a figure representing lipidomics and proteomics data. Colorblind-friendly palettes were applied to the relative abundance values and mapped to a static image displaying lipid metabolism pathways. The script was written in Perl using the GD graphics package.

## DATA AND SOFTWARE AVAILABILITY

Proteomics data were deposited into Pride repository (www.ebi.ac.uk/pride) under accession number PXD017734.

Username: reviewer86800@ebi.ac.uk

Password: 9cZs0O1G

The code for the lipidomics visualization tool is available under the BSD 2-Clause License at GitHub under URL: https://github.com/wichne/LipidomicsMapTools

## AUTHOR CONTRIBUTIONS

D.Z.M., H.M.H., M.C.B., J.D.N and E.S.N. designed the research. D.Z.M. performed the *H. capsulatum* growth, drug testing and cytokine experiments. H.M.H., M.C.B., E.M.Z., J.E.K., K.K.W., E.L.B. and K.J.B. performed the lipidomics and proteomics experiments. E.L.B. performed the genetic engineering of the *S. cerevisiae* strains. M.C.B., H.M.H., N.M.M. and Y.M.K. performed the gas chromatography-mass spectrometry analyses. E.S.N., G.C., J.D.Z., J.R.T. build the lipid metabolic map. W.C.N. developed the lipidomics/proteomics visualization tool. X.Z. and E.S.B. performed the ion mobility-mass spectrometry analysis. M.R.G. performed the platelet aggregation analysis. D.Z.M., H.M.H., M.C.B., S.P.C., X.Z., E.S.B, J.E.K., S.H.P., Y.M.K., M.R.G., J.D.N., and E.S.N. analyzed the data. M.R.G., E.S.B, S.H.P., J.D.N and E.S.N. contributed with reagents and resources. D.Z.M., H.M.H, M.C.B. and E.S.N. wrote the manuscript with inputs from the other authors. All the authors read and approved the final version of the manuscript.

## CONFLICTS OF INTEREST

The authors declare no financial conflicts of interest.


## Acknowledgments

The authors thank Drs. Igor Almeida, Rosa Maldonado, Milene Carmes Vallejo, Charles Ansong and Joshua Adkins for insightful discussions. Joshua D. Nosanchuk and Ernesto S. Nakayasu were supported by NIH R21 AI124797. Erin L. Bredeweg, Ernesto S. Nakayasu, Jennifer Kyle were supported by a Laboratory Directed Research and Development project from Pacific Northwest National Laboratory (PNNL). Erin S. Baker would also like to acknowledge support from NIEHS P42 ES027704. Parts of this work were performed in the Environmental Molecular Science Laboratory, a U.S. Department of Energy (DOE) national scientific user facility at PNNL in Richland, WA.

## References


Albuquerque, P.C., Nakayasu, E.S., Rodrigues, M.L., Frases, S., Casadevall, A., Zancope-Oliveira, R.M., Almeida, I.C., and Nosanchuk, J.D. (2008). Vesicular transport in Histoplasma capsulatum: an effective mechanism for trans-cell wall transfer of proteins and lipids in ascomycetes. Cell Microbiol *10*, 1695-1710.

Alloatti, A., Testero, S.A., and Uttaro, A.D. (2009). Chemical evaluation of fatty acid desaturases as drug targets in Trypanosoma cruzi. Int J Parasitol *39*, 985-993.

Anderson, T.M., Clay, M.C., Cioffi, A.G., Diaz, K.A., Hisao, G.S., Tuttle, M.D., Nieuwkoop, A.J., Comellas, G., Maryum, N., Wang, S.*, et al.* (2014). Amphotericin forms an extramembranous and fungicidal sterol sponge. Nat Chem Biol *10*, 400-406.

Antinori, S. (2014). Histoplasma capsulatum: more widespread than previously thought. Am J Trop Med Hyg *90*, 982-983.

Armstrong, P.A., Jackson, B.R., Haselow, D., Fields, V., Ireland, M., Austin, C., Signs, K., Fialkowski, V., Patel, R., Ellis, P.*, et al.* (2018). Multistate Epidemiology of Histoplasmosis, United States, 2011-2014. Emerg Infect Dis *24*, 425-431.

Artunduaga Bonilla, J.J., Honorato, L., Haranahalli, K., Gremiao, I.D.F., Pereira, S.A., Guimaraes, A., Baptista, A.R.S., de, M.T.P., Rodrigues, M.L., Miranda, K.*, et al.* (2021). Antifungal activity of Acylhydrazone derivatives against Sporothrix spp. Antimicrob Agents Chemother.

Baltazar, L.M., Zamith-Miranda, D., Burnet, M.C., Choi, H., Nimrichter, L., Nakayasu, E.S., and Nosanchuk, J.D. (2018). Concentration-dependent protein loading of extracellular vesicles released by Histoplasma capsulatum after antibody treatment and its modulatory action upon macrophages. Sci Rep *8*, 8065.

Beck, M., Schmidt, A., Malmstroem, J., Claassen, M., Ori, A., Szymborska, A., Herzog, F., Rinner, O., Ellenberg, J., and Aebersold, R. (2011). The quantitative proteome of a human cell line. Mol Syst Biol *7*, 549.

Benedict, K., and Mody, R.K. (2016). Epidemiology of Histoplasmosis Outbreaks, United States, 1938-2013. Emerg Infect Dis *22*, 370-378.

Bongomin, F., Gago, S., Oladele, R.O., and Denning, D.W. (2017). Global and Multi-National Prevalence of Fungal Diseases-Estimate Precision. J Fungi (Basel) *3*.

Burnet, M.C., Zamith-Miranda, D., Heyman, H.M., Weitz, K.K., Bredeweg, E.L., Nosanchuk, J.D., and Nakayasu, E.S. (2020). Remodeling of the Histoplasma Capsulatum Membrane Induced by Monoclonal Antibodies. Vaccines (Basel) *8*.

Caretti, A., Torelli, R., Perdoni, F., Falleni, M., Tosi, D., Zulueta, A., Casas, J., Sanguinetti, M., Ghidoni, R., Borghi, E.*, et al.* (2016). Inhibition of ceramide de novo synthesis by myriocin produces the double effect of reducing pathological inflammation and exerting antifungal activity against A. fumigatus airways infection. Biochim Biophys Acta *1860*, 1089-1097.

Carratu, L., Franceschelli, S., Pardini, C.L., Kobayashi, G.S., Horvath, I., Vigh, L., and Maresca, B. (1996). Membrane lipid perturbation modifies the set point of the temperature of heat shock response in yeast. Proc Natl Acad Sci U S A *93*, 3870-3875.

Casanovas, A., Sprenger, R.R., Tarasov, K., Ruckerbauer, D.E., Hannibal-Bach, H.K., Zanghellini, J., Jensen, O.N., and Ejsing, C.S. (2015). Quantitative analysis of proteome and lipidome dynamics reveals functional regulation of global lipid metabolism. Chem Biol *22*, 412-425.

Chaithra, V.H., Jacob, S.P., Lakshmikanth, C.L., Sumanth, M.S., Abhilasha, K.V., Chen, C.H., Thyagarajan, A., Sahu, R.P., Travers, J.B., McIntyre, T.M.*, et al.* (2018). Modulation of inflammatory platelet-activating factor (PAF) receptor by the acyl analogue of PAF. J Lipid Res *59*, 2063-2074.

Chu, J.H., Feudtner, C., Heydon, K., Walsh, T.J., and Zaoutis, T.E. (2006). Hospitalizations for endemic mycoses: a population-based national study. Clin Infect Dis *42*, 822-825.

Cleare, L.G., Zamith, D., Heyman, H.M., Couvillion, S.P., Nimrichter, L., Rodrigues, M.L., Nakayasu, E.S., and Nosanchuk, J.D. (2020). Media matters! Alterations in the loading and

release of Histoplasma capsulatum extracellular vesicles in response to different nutritional milieus. Cell Microbiol, e13217.
Damude, H.G., Zhang, H., Farrall, L., Ripp, K.G., Tomb, J.F., Hollerbach, D., and Yadav, N.S. (2006). Identification of bifunctional delta12/omega3 fatty acid desaturases for improving the ratio of omega3 to omega6 fatty acids in microbes and plants. Proc Natl Acad Sci U S A *103*, 9446-9451.
Dautel, S.E., Kyle, J.E., Clair, G., Sontag, R.L., Weitz, K.K., Shukla, A.K., Nguyen, S.N., Kim, Y.M., Zink, E.M., Luders, T.*, et al.* (2017). Lipidomics reveals dramatic lipid compositional changes in the maturing postnatal lung. Sci Rep *7*, 40555.
de Melo, N.R., Abdrahman, A., Greig, C., Mukherjee, K., Thornton, C., Ratcliffe, N.A., Vilcinskas, A., and Butt, T.M. (2013). Myriocin significantly increases the mortality of a non-mammalian model host during Candida pathogenesis. PLoS One *8*, e78905.
Deepe, G.S., Jr., and Buesing, W.R. (2012). Deciphering the pathways of death of Histoplasma capsulatum-infected macrophages: implications for the immunopathogenesis of early infection. J Immunol *188*, 334-344.
Domer, J.E., and Hamilton, J.G. (1971). The readily extracted lipids of Histoplasma capsulatum and Blastomyces dermatitidis. Biochim Biophys Acta *231*, 465-478.
Femia, E.A., Scavone, M., Lecchi, A., and Cattaneo, M. (2013). Effect of platelet count on platelet aggregation measured with impedance aggregometry (Multiplate analyzer) and with light transmission aggregometry. J Thromb Haemost *11*, 2193-2196.
Fradin, C., Bernardes, E.S., and Jouault, T. (2015). Candida albicans phospholipomannan: a sweet spot for controlling host response/inflammation. Semin Immunopathol *37*, 123-130.
Gao, J., Wang, H., Li, Z., Wong, A.H., Wang, Y.Z., Guo, Y., Lin, X., Zeng, G., Liu, H., Wang, Y.*, et al.* (2018). Candida albicans gains azole resistance by altering sphingolipid composition. Nat Commun *9*, 4495.
Gargano, S., Di Lallo, G., Kobayashi, G.S., and Maresca, B. (1995). A temperature-sensitive strain of *Histoplasma capsulatum* has an altered delta 9-fatty acid desaturase gene. Lipids *30*, 899-906.
Ghannoum, M.A., and Rice, L.B. (1999). Antifungal agents: mode of action, mechanisms of resistance, and correlation of these mechanisms with bacterial resistance. Clin Microbiol Rev *12*, 501-517.
Gietz, R.D., Schiestl, R.H., Willems, A.R., and Woods, R.A. (1995). Studies on the transformation of intact yeast cells by the LiAc/SS-DNA/PEG procedure. Yeast *11*, 355-360.
Goughenour, K.D., and Rappleye, C.A. (2017). Antifungal therapeutics for dimorphic fungal pathogens. Virulence *8*, 211-221.
Gray, K.C., Palacios, D.S., Dailey, I., Endo, M.M., Uno, B.E., Wilcock, B.C., and Burke, M.D. (2012). Amphotericin primarily kills yeast by simply binding ergosterol. Proc Natl Acad Sci U S A *109*, 2234-2239.
Guimaraes, L.L., Toledo, M.S., Ferreira, F.A., Straus, A.H., and Takahashi, H.K. (2014). Structural diversity and biological significance of glycosphingolipids in pathogenic and opportunistic fungi. Front Cell Infect Microbiol *4*, 138.
Hartmann, A., and Jozefowicz, A.M. (2018). VANTED: A Tool for Integrative Visualization and Analysis of -Omics Data. Methods Mol Biol *1696*, 261-278.
Hiller, K., Hangebrauk, J., Jager, C., Spura, J., Schreiber, K., and Schomburg, D. (2009). MetaboliteDetector: comprehensive analysis tool for targeted and nontargeted GC/MS based metabolome analysis. Anal Chem *81*, 3429-3439.
Hogan, L.H., Klein, B.S., and Levitz, S.M. (1996). Virulence factors of medically important fungi. Clin Microbiol Rev *9*, 469-488.
Kim, Y.M., Schmidt, B.J., Kidwai, A.S., Jones, M.B., Deatherage Kaiser, B.L., Brewer, H.M., Mitchell, H.D., Palsson, B.O., McDermott, J.E., Heffron, F.*, et al.* (2013). Salmonella modulates

metabolism during growth under conditions that induce expression of virulence genes. Mol Biosyst *9*, 1522-1534.
Kind, T., Wohlgemuth, G., Lee, D.Y., Lu, Y., Palazoglu, M., Shahbaz, S., and Fiehn, O. (2009). FiehnLib: mass spectral and retention index libraries for metabolomics based on quadrupole and time-of-flight gas chromatography/mass spectrometry. Anal Chem *81*, 10038-10048.
Kluepfel, D., Bagli, J., Baker, H., Charest, M.P., and Kudelski, A. (1972). Myriocin, a new antifungal antibiotic from Myriococcum albomyces. J Antibiot (Tokyo) *25*, 109-115.
Lazzarini, C., Haranahalli, K., Rieger, R., Ananthula, H.K., Desai, P.B., Ashbaugh, A., Linke, M.J., Cushion, M.T., Ruzsicska, B., Haley, J.*, et al.* (2018). Acylhydrazones as Antifungal Agents Targeting the Synthesis of Fungal Sphingolipids. Antimicrob Agents Chemother *62*.
Levery, S.B., Toledo, M.S., Straus, A.H., and Takahashi, H.K. (2001). Comparative analysis of glycosylinositol phosphorylceramides from fungi by electrospray tandem mass spectrometry with low-energy collision-induced dissociation of Li(+) adduct ions. Rapid Commun Mass Spectrom *15*, 2240-2258.
Maldonado, R.A., Kuniyoshi, R.K., Linss, J.G., and Almeida, I.C. (2006). Trypanosoma cruzi oleate desaturase: molecular characterization and comparative analysis in other trypanosomatids. J Parasitol *92*, 1064-1074.
Maresca, B., and Kobayashi, G. (1993). Changes in membrane fluidity modulate heat shock gene expression and produced attenuated strains in the dimorphic fungus *Histoplasma capsulatum*. Archives of medical research *24*, 247-249.
Matos Baltazar, L., Nakayasu, E.S., Sobreira, T.J., Choi, H., Casadevall, A., Nimrichter, L., and Nosanchuk, J.D. (2016). Antibody Binding Alters the Characteristics and Contents of Extracellular Vesicles Released by Histoplasma capsulatum. mSphere *1*.
Medeiros, A.I., Secatto, A., Belanger, C., Sorgi, C.A., Borgeat, P., Marleau, S., and Faccioli, L.H. (2015). Impairment of neutrophil migration to remote inflammatory site during lung histoplasmosis. Biomed Res Int *2015*, 409309.
Merrill, A.H., Jr. (2011). Sphingolipid and glycosphingolipid metabolic pathways in the era of sphingolipidomics. Chem Rev *111*, 6387-6422.
Metzl-Raz, E., Kafri, M., Yaakov, G., Soifer, I., Gurvich, Y., and Barkai, N. (2017). Principles of cellular resource allocation revealed by condition-dependent proteome profiling. Elife *6*.
Mor, V., Rella, A., Farnoud, A.M., Singh, A., Munshi, M., Bryan, A., Naseem, S., Konopka, J.B., Ojima, I., Bullesbach, E.*, et al.* (2015). Identification of a New Class of Antifungals Targeting the Synthesis of Fungal Sphingolipids. MBio *6*, e00647.
Munshi, M.A., Gardin, J.M., Singh, A., Luberto, C., Rieger, R., Bouklas, T., Fries, B.C., and Del Poeta, M. (2018). The Role of Ceramide Synthases in the Pathogenicity of *Cryptococcus neoformans*. Cell reports *22*, 1392-1400.
Nakayama, R., Kumagai, H., and Saito, K. (1994). Evidence for production of platelet-activating factor by yeast Saccharomyces cerevisiae cells. Biochim Biophys Acta *1199*, 137-142.
Nakayasu, E.S., Nicora, C.D., Sims, A.C., Burnum-Johnson, K.E., Kim, Y.M., Kyle, J.E., Matzke, M.M., Shukla, A.K., Chu, R.K., Schepmoes, A.A.*, et al.* (2016). MPLEx: a Robust and Universal Protocol for Single-Sample Integrative Proteomic, Metabolomic, and Lipidomic Analyses. mSystems *1*.
Nguyen, L.N., Gacser, A., and Nosanchuk, J.D. (2011). The stearoyl-coenzyme A desaturase 1 is essential for virulence and membrane stress in Candida parapsilosis through unsaturated fatty acid production. Infect Immun *79*, 136-145.
Nguyen, L.N., Trofa, D., and Nosanchuk, J.D. (2009). Fatty acid synthase impacts the pathobiology of Candida parapsilosis in vitro and during mammalian infection. PLoS One *4*, e8421.
Nielsen, H.S. (1966). Variation in Lipid Content of Strains of *Histoplasma capsulatum* Exhibiting Different Virulence Properties for Mice. Journal of bacteriology *91*, 273-277.

O'Meara, T.R., Duah, K., Guo, C.X., Maxson, M.E., Gaudet, R.G., Koselny, K., Wellington, M., Powers, M.E., MacAlpine, J., O'Meara, M.J.*, et al.* (2018). High-Throughput Screening Identifies Genes Required for Candida albicans Induction of Macrophage Pyroptosis. MBio *9*.
Palacios, D.S., Dailey, I., Siebert, D.M., Wilcock, B.C., and Burke, M.D. (2011). Synthesis-enabled functional group deletions reveal key underpinnings of amphotericin B ion channel and antifungal activities. Proc Natl Acad Sci U S A *108*, 6733-6738.
Parente-Rocha, J.A., Bailao, A.M., Amaral, A.C., Taborda, C.P., Paccez, J.D., Borges, C.L., and Pereira, M. (2017). Antifungal Resistance, Metabolic Routes as Drug Targets, and New Antifungal Agents: An Overview about Endemic Dimorphic Fungi. Mediators Inflamm *2017*, 9870679.
Perdoni, F., Signorelli, P., Cirasola, D., Caretti, A., Galimberti, V., Biggiogera, M., Gasco, P., Musicanti, C., Morace, G., and Borghi, E. (2015). Antifungal activity of Myriocin on clinically relevant Aspergillus fumigatus strains producing biofilm. BMC Microbiol *15*, 248.
Pettersen, R.J., Salem, M., Skorve, J., Ulvik, R.J., Berge, R.K., and Nordrehaug, J.E. (2008). Pharmacology and safety of tetradecylthioacetic acid (TTA): phase-1 study. J Cardiovasc Pharmacol *51*, 410-417.
Phetsuksiri, B., Baulard, A.R., Cooper, A.M., Minnikin, D.E., Douglas, J.D., Besra, G.S., and Brennan, P.J. (1999). Antimycobacterial activities of isoxyl and new derivatives through the inhibition of mycolic acid synthesis. Antimicrob Agents Chemother *43*, 1042-1051.
Phetsuksiri, B., Jackson, M., Scherman, H., McNeil, M., Besra, G.S., Baulard, A.R., Slayden, R.A., DeBarber, A.E., Barry, C.E., 3rd, Baird, M.S.*, et al.* (2003). Unique mechanism of action of the thiourea drug isoxyl on Mycobacterium tuberculosis. J Biol Chem *278*, 53123-53130.
Pianalto, K.M., and Alspaugh, J.A. (2016). New Horizons in Antifungal Therapy. J Fungi (Basel) *2*.
Pluskal, T., Castillo, S., Villar-Briones, A., and Oresic, M. (2010). MZmine 2: modular framework for processing, visualizing, and analyzing mass spectrometry-based molecular profile data. BMC Bioinformatics *11*, 395.
Prescott, S.M., Zimmerman, G.A., Stafforini, D.M., and McIntyre, T.M. (2000). Platelet-activating factor and related lipid mediators. Annu Rev Biochem *69*, 419-445.
Radovanovic, N., Thambugala, D., Duguid, S., Loewen, E., and Cloutier, S. (2014). Functional characterization of flax fatty acid desaturase FAD2 and FAD3 isoforms expressed in yeast reveals a broad diversity in activity. Mol Biotechnol *56*, 609-620.
Rella, A., Farnoud, A.M., and Del Poeta, M. (2016). Plasma membrane lipids and their role in fungal virulence. Prog Lipid Res *61*, 63-72.
Rittershaus, P.C., Kechichian, T.B., Allegood, J.C., Merrill, A.H., Jr., Hennig, M., Luberto, C., and Del Poeta, M. (2006). Glucosylceramide synthase is an essential regulator of pathogenicity of Cryptococcus neoformans. J Clin Invest *116*, 1651-1659.
Siafakas, A.R., Wright, L.C., Sorrell, T.C., and Djordjevic, J.T. (2006). Lipid rafts in Cryptococcus neoformans concentrate the virulence determinants phospholipase B1 and Cu/Zn superoxide dismutase. Eukaryot Cell *5*, 488-498.
Singh, A., Wang, H., Silva, L.C., Na, C., Prieto, M., Futerman, A.H., Luberto, C., and Del Poeta, M. (2012). Methylation of glycosylated sphingolipid modulates membrane lipid topography and pathogenicity of Cryptococcus neoformans. Cell Microbiol *14*, 500-516.
Spitzer, M., Griffiths, E., Blakely, K.M., Wildenhain, J., Ejim, L., Rossi, L., De Pascale, G., Curak, J., Brown, E., Tyers, M.*, et al.* (2011). Cross-species discovery of syncretic drug combinations that potentiate the antifungal fluconazole. Mol Syst Biol *7*, 499.
Strader, C.R., Pearce, C.J., and Oberlies, N.H. (2011). Fingolimod (FTY720): a recently approved multiple sclerosis drug based on a fungal secondary metabolite. J Nat Prod *74*, 900-907.
Tagliari, L., Toledo, M.S., Lacerda, T.G., Suzuki, E., Straus, A.H., and Takahashi, H.K. (2012). Membrane microdomain components of Histoplasma capsulatum yeast forms, and their role in alveolar macrophage infectivity. Biochim Biophys Acta *1818*, 458-466.

Tamaki, H., Shimada, A., Ito, Y., Ohya, M., Takase, J., Miyashita, M., Miyagawa, H., Nozaki, H., Nakayama, R., and Kumagai, H. (2007). LPT1 encodes a membrane-bound O-acyltransferase involved in the acylation of lysophospholipids in the yeast Saccharomyces cerevisiae. J Biol Chem *282*, 34288-34298.
Toledo, M.S., Levery, S.B., Suzuki, E., Straus, A.H., and Takahashi, H.K. (2001). Characterization of cerebrosides from the thermally dimorphic mycopathogen Histoplasma capsulatum: expression of 2-hydroxy fatty N-acyl (E)-Delta(3)-unsaturation correlates with the yeast-mycelium phase transition. Glycobiology *11*, 113-124.
Tousek, J. (1970). On the clinical effectiveness of Isoxyl. Antibiot Chemother *16*, 149-155.
Urbancik, B. (1970). Clinical experience with thiocarlide (Isoxyl). Antibiot Chemother *16*, 117-123.
Vallejo, M.C., Nakayasu, E.S., Longo, L.V., Ganiko, L., Lopes, F.G., Matsuo, A.L., Almeida, I.C., and Puccia, R. (2012). Lipidomic analysis of extracellular vesicles from the pathogenic phase of Paracoccidioides brasiliensis. PLoS One *7*, e39463.
Wang, C., and Hickey, A.J. (2010). Isoxyl particles for pulmonary delivery: In vitro cytotoxicity and potency. Int J Pharm *396*, 99-104.
Weete, J.D., Abril, M., and Blackwell, M. (2010). Phylogenetic distribution of fungal sterols. PLoS One *5*, e10899.
Wilhelm, M., Schlegl, J., Hahne, H., Gholami, A.M., Lieberenz, M., Savitski, M.M., Ziegler, E., Butzmann, L., Gessulat, S., Marx, H.*, et al.* (2014). Mass-spectrometry-based draft of the human proteome. Nature *509*, 582-587.
Zamith-Miranda, D., Heyman, H.M., Cleare, L.G., Couvillion, S.P., Clair, G.C., Bredeweg, E.L., Gacser, A., Nimrichter, L., Nakayasu, E.S., and Nosanchuk, J.D. (2019). Multi-omics Signature of Candida auris, an Emerging and Multidrug-Resistant Pathogen. mSystems *4*.
Zarnowski, R., Dobrzyn, A., Ntambi, J.M., and Woods, J.P. (2008). Neutral storage lipids of *Histoplasma capsulatum*: effect of culture age. Curr Microbiol *56*, 110-114.
Zhang, X., Romm, M., Zheng, X., Zink, E.M., Kim, Y.M., Burnum-Johnson, K.E., Orton, D.J., Apffel, A., Ibrahim, Y.M., Monroe, M.E.*, et al.* (2016). SPE-IMS-MS: An automated platform for sub-sixty second surveillance of endogenous metabolites and xenobiotics in biofluids. Clin Mass Spectrom *2*, 1-10.

**Figure 1**

**A**

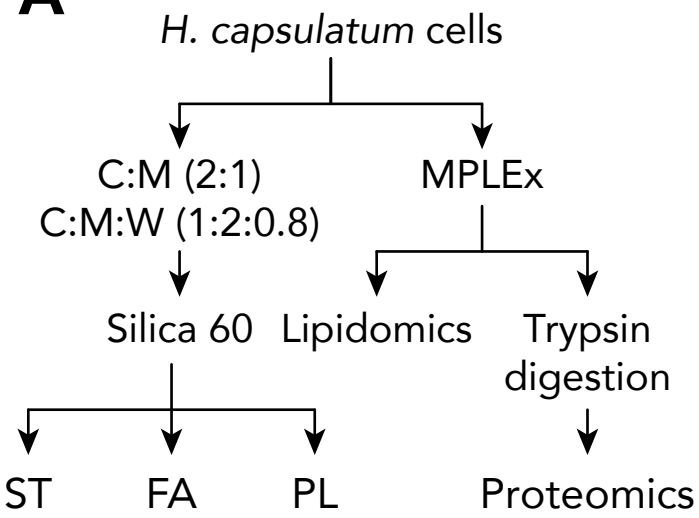


**B**

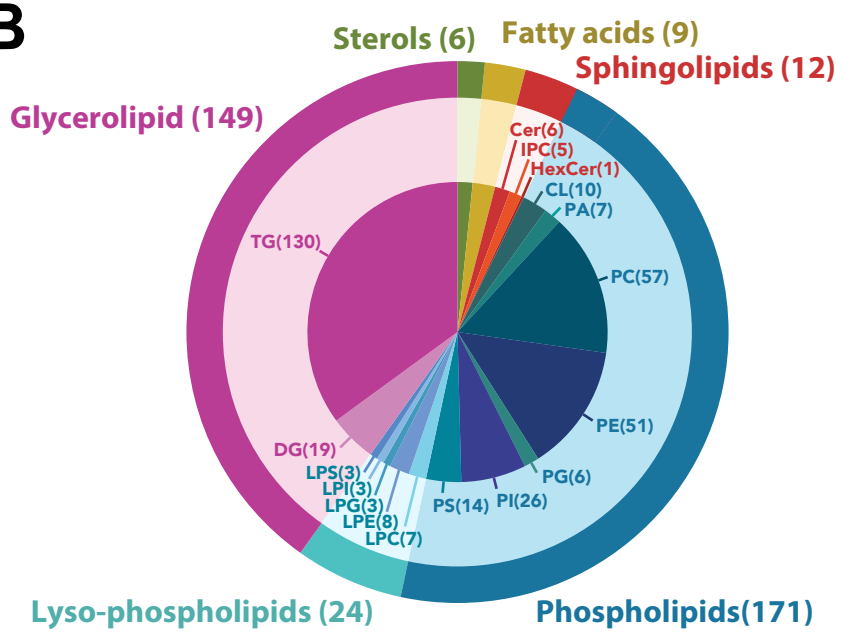


**TOTAL: 371 species**

**C**

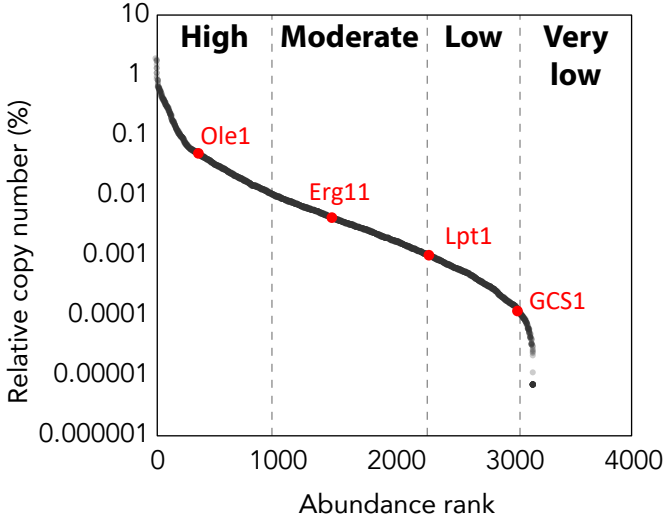


**D**

| | Fold Enrichment | | | |
|---|---|---|---|---|
| Pathway | High | Moderate | Low | Very Low |
| Glycolysis / Gluconeogenesis | **5.9** | 1.1 | 0.0 | 0.0 |
| Citrate cycle (TCA cycle) | **8.7** | 0.0 | 0.0 | 0.0 |
| DNA replication | 1.3 | **3.9** | **2.4** | 2.3 |
| Nicotinate and nicotinamide metabolism | 0.6 | 1.7 | **4.1** | 0.0 |
| Basal transcription factors | 0.3 | **2.4** | **4.4** | **7.0** |
| Fatty acid metabolism | **4.5** | 1.6 | 0.4 | 0.0 |
| Fatty acid biosynthesis | **3.8** | 1.4 | 0.0 | 0.0 |
| Fatty acid elongation | **4.7** | 1.8 | 1.5 | 0.0 |
| Fatty acid degradation | **5.5** | 1.2 | 0.0 | 0.0 |
| Arachidonic acid metabolism | 4.7 | 0.0 | 0.0 | 0.0 |
| alpha-Linolenic acid metabolism | 1.6 | 1.2 | 0.0 | 0.0 |
| Biosynthesis of unsaturated fatty acids | **3.1** | 1.8 | 0.0 | 0.0 |
| Steroid biosynthesis | 1.7 | **2.9** | 1.6 | 0.0 |
| Glycerophospholipid metabolism | 0.5 | **2.2** | **2.7** | 3.4 |
| Ether lipid metabolism | 0.9 | 0.6 | **6.4** | 0.0 |
| Sphingolipid metabolism | 1.4 | 2.2 | 1.8 | 0.0 |
| Glycosylphosphatidylinositol (GPI)-anchor biosynthesis | 0.0 | 1.5 | 1.2 | 0.0 |

**Figure 1. Proteomic and lipidomic analyses of *Histoplasma capsulatum* yeast cells.**
(**A**) Extraction procedure for lipidomics proteomics analyses. Yeast cells were extracted sequentially with chloroform:methanol (2:1, v:v) and chloroform:methanol:water (1:2:0.8, v:v:) and fractionated by Silica 60 solid phase extraction for sterol, free fatty acid and phospholipid analyses. Cells were also submitted to simultaneous metabolite, protein and lipid extraction (MPLEx) for global lipidomics and proteomics analyses.
(**B**) Overall lipid coverage combining MPLEx and specific lipid extractions of *Histoplasma capsulatum*.
(**C**) Protein abundance classification based on their relative copy numbers.
(**D**) Function enrichment analysis based on the KEGG annotation of *H. capsulatum* proteins with different abundance levels.
Abbreviations: C, chloroform; Cer, ceramide; CL, cardiolipin; DG, diacylglycerol; FA, fatty acid; HexCer, hexosylceramide; LPC, lysophosphatidylcholine, LPE, lysophosphatidylethanolamines, LPG, lysophosphatidylglycerol; LPI, lysophosphatidylinositol; LPS, lysophosphatidylserine; M, methanol; PA, phosphatidic acid; PC, phosphatidylinositol; PE, phosphatidylethanolamine; PG, phosphatidylglycerol; PI, phosphatidylinositol; PI_Cer, inositolphosphoceramide; PL, phospholipid; PS, phosphatidylserine; ST, sterol; TG, triacylglycerol; W, water.

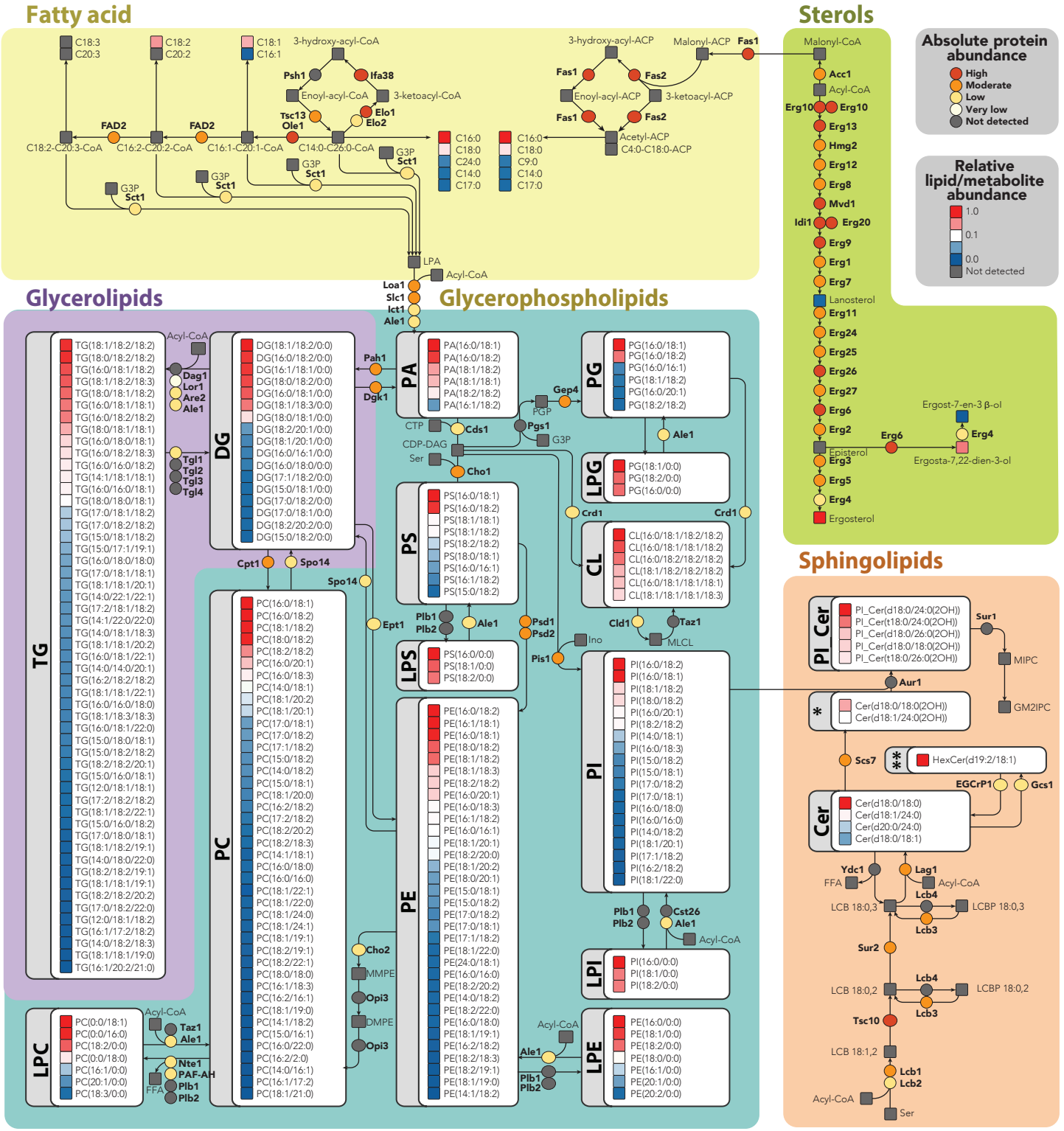


Figure 2

* Cer(2OH) ** HexCer

**Figure 2. Metabolic map of *Histoplasma capsulatum* lipids and biosynthesis proteins.**

The map was built based on genomic information along with proteomics and lipidomics data. Lipids abundances were normalized by the most intense signal in the mass spectrometry analysis within each lipid class, whereas the proteins were quantified based on their relative copy number. For details about enzyme names and homologs see table **S10**. Abbreviations: Cer, ceramide; CL, cardiolipin; DG, diacylglycerol; HexCer, hexosylceramide; LPC, lysophosphatidylcholine, LPE, lysophosphatidylethanolamines, LPG, lysophosphatidylglycerol; LPI, lysophosphatidylinositol; LPS, lysophosphatidylserine; M, methanol; PA, phosphatidic acid; PC, phosphatidylinositol; PE, phosphatidylethanolamine; PG, phosphatidylglycerol; PI, phosphatidylinositol; PI_Cer, inositolphosphoceramide; PL, phospholipid; PS, phosphatidylserine; TG, triacylglycerol.

Figure 3

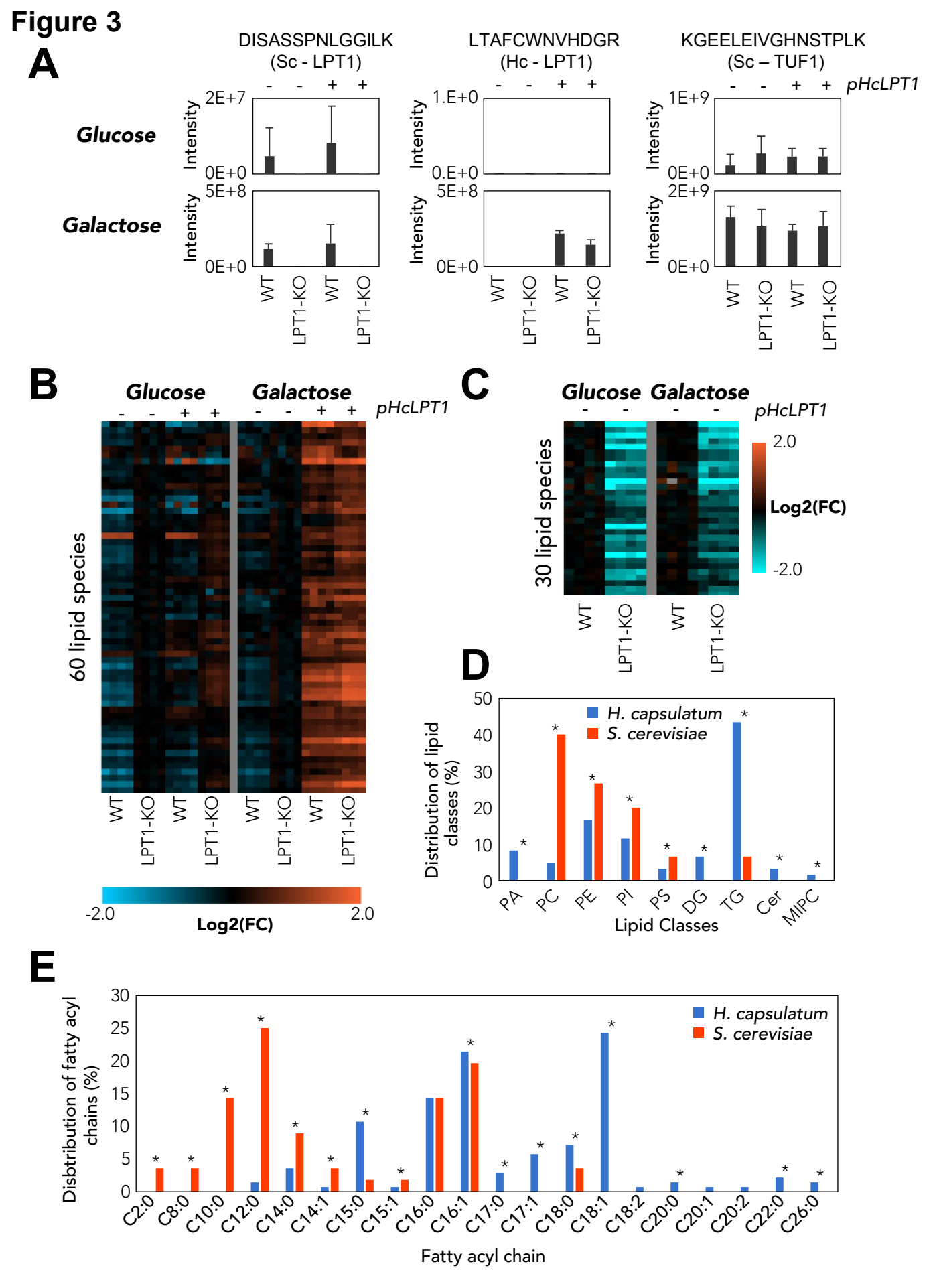
A
DISASSPNLGGILK
(Sc - LPT1)
LTAFCWNVHDGR
(Hc - LPT1)
KGEELEIVGHNSTPLK
(Sc – TUF1)
pHcLPT1
Glucose
Galactose
Intensity
2E+7
0E+0
1.E+0
0.E+0
1E+9
5E+8
2E+9
WT
LPT1-KO
B
Glucose
Galactose
pHcLPT1
60 lipid species
Log2(FC)
-2.0
2.0
C
30 lipid species
D
H. capsulatum
S. cerevisiae
Distribution of lipid classes (%)
PA
PC
PE
PI
PS
DG
TG
Cer
MIPC
Lipid Classes
E
Disbtribution of fatty acyl chains (%)
C2:0
C8:0
C10:0
C12:0
C14:0
C14:1
C15:0
C15:1
C16:0
C16:1
C17:0
C17:1
C18:0
C18:1
C18:2
C20:0
C20:1
C20:2
C22:0
C26:0
Fatty acyl chain

**Figure 3. Analysis of *Saccharomyces cerevisiae* (Sc) and *Histoplasma capsulatum* (Hc) lysophospholipid acetyltransferase LPT1 genes.**

The analysis was done in wild-type and LPT1-knockout (KO) (*Lpt1* -/-) *S. cerevisiae* strains complemented or not with the pESC-URA plasmid with Hc-LPT1 gene under galactose-inducible promoter. *S. cerevisiae* WT and LPT1-knockout (KO) strains were grown in YNB medium supplemented with glucose (Glc) or galactose (Gal).

(**A**) Protein abundance of Sc and Hc LPT1 proteins measured by the intensity of specific peptides in the LC-MS/MS analysis. Elongation factor Tu (TUF1) was used as a loading control. As expected, Sc LPT1 was only detected in the WT strain, whereas Hc LPT1 was detected only in strains transformed with the plasmid and induced with galactose.

(**B-C**) Heatmaps of identified HcLPT1 (**B**) and ScLPT1 (**C**) products ($p \leq 0.05$ compared the complemented vs control strains (**B**) or LPT1-KO vs. WT strains (**C**). The experiments were done in two independent batches delimited by the vertical grey lines.

(**D-E**) Distribution of the lipid classes (**D**) and fatty acyl groups (**E**) of the HcLPT1 and ScLPT1 products. *$p \leq 0.05$ by Fisher's exact test.

Figure 4

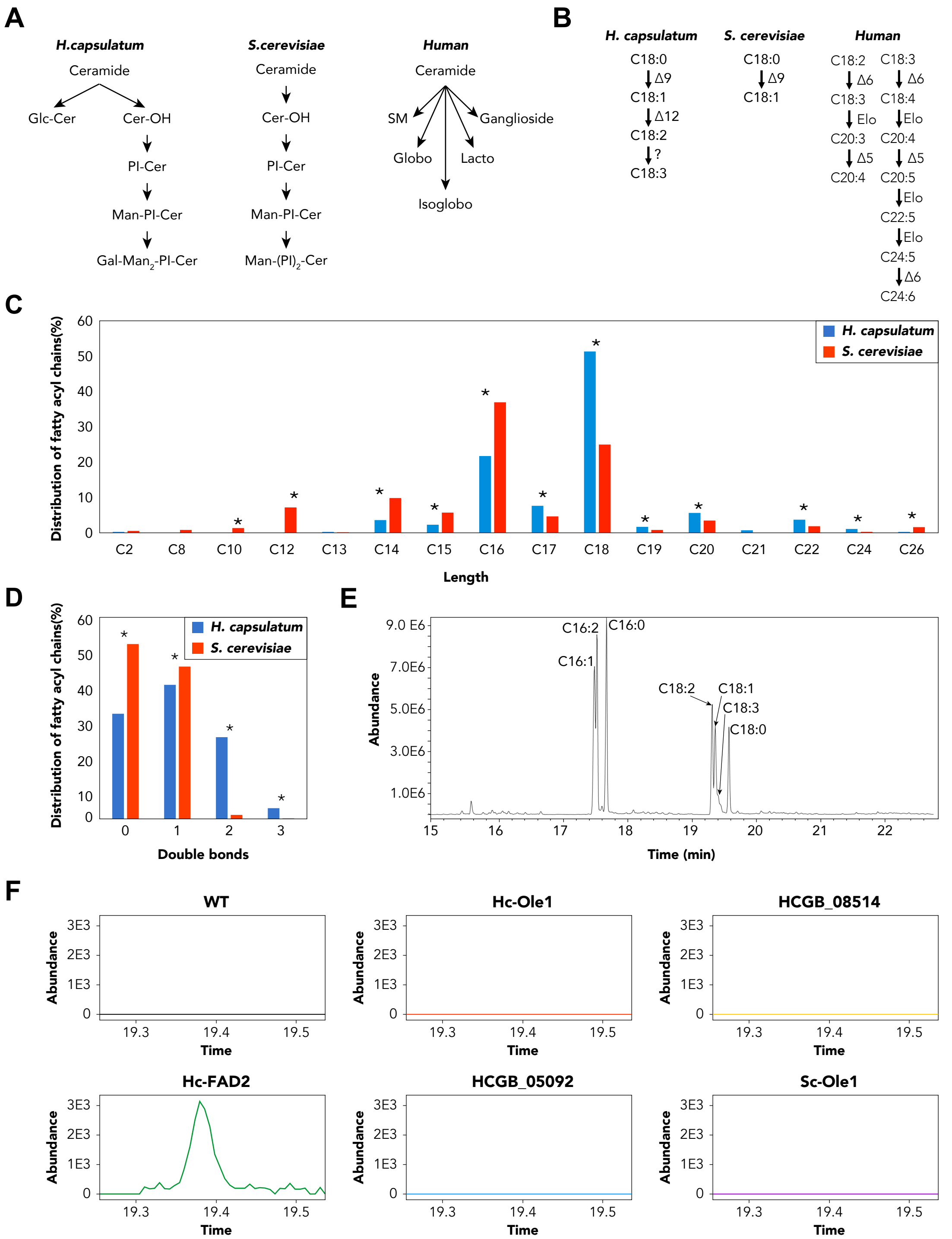
A
H.capsulatum
Ceramide
Glc-Cer
Cer-OH
PI-Cer
Man-PI-Cer
Gal-Man2-PI-Cer
S.cerevisiae
Ceramide
Cer-OH
PI-Cer
Man-PI-Cer
Man-(PI)2-Cer
Human
Ceramide
SM
Ganglioside
Globo
Lacto
Isoglobo
B
H. capsulatum
C18:0
Δ9
C18:1
Δ12
C18:2
?
C18:3
S. cerevisiae
C18:0
Δ9
C18:1
Human
C18:2
Δ6
C18:3
Elo
C20:3
Δ5
C20:4
C18:3
Δ6
C18:4
Elo
C20:4
Δ5
C20:5
Elo
C22:5
Elo
C24:5
Δ6
C24:6
C
Distribution of fatty acyl chains(%)
H. capsulatum
S. cerevisiae
C2
C8
C10
C12
C13
C14
C15
C16
C17
C18
C19
C20
C21
C22
C24
C26
Length
D
Distribution of fatty acyl chains(%)
H. capsulatum
S. cerevisiae
Double bonds
E
Abundance
C16:2
C16:0
C16:1
C18:2
C18:1
C18:3
C18:0
Time (min)
F
WT
Hc-Ole1
HCGB_08514
Hc-FAD2
HCGB_05092
Sc-Ole1
Abundance
Time

**Figure 4. Sphingolipid and fatty acid metabolism in *Histoplasma capsulatum*.**
(**A**) Sphingolipids of *H. capsulatum*, *Saccharomyces cerevisiae* and humans.
(**B**) Fatty acid desaturase pathways in *H. capsulatum*, *S. cerevisiae* and humans.
(**C**) Distribution of carbon chain lengths of fatty acyl groups from lipids in global lipidomic analysis.
(**D**) Distribution of double bonds on fatty acyl groups from lipids in global lipidomic analysis.
(**E**) Representative chromatogram of fatty acid analysis from *S. cerevisiae* cells expressing *H. capsulatum* FAD2 gene. The analysis was done in *S. cerevisiae* strain transformed with the pESC-URA plasmid with Hc-FAD2 gene under galactose-inducible promoter. Cells were grown in YNB medium supplemented with galactose. The chromatogram shows the production of fatty acids with 2 and 3 double bonds.
(F) Extracted ion chromatogram of α-linolenic acid (C18:3 – 9Z, 12Z, 15Z) of *S. cerevisiae* cells expressing various fatty acid desaturase candidates. α-linolenic acid was only detected in cells expressing the *H. capsulatum* FAD2 gene,
Statistical test: *$p \leq 0.05$ by Fisher's exact test.

A

| Drug | MIC (μM) |
|---|---|
| 10-Thiastearic acid | 1.25 |
| Thiocarlide | 12.5 |
| Myriocin | 0.03 |

B

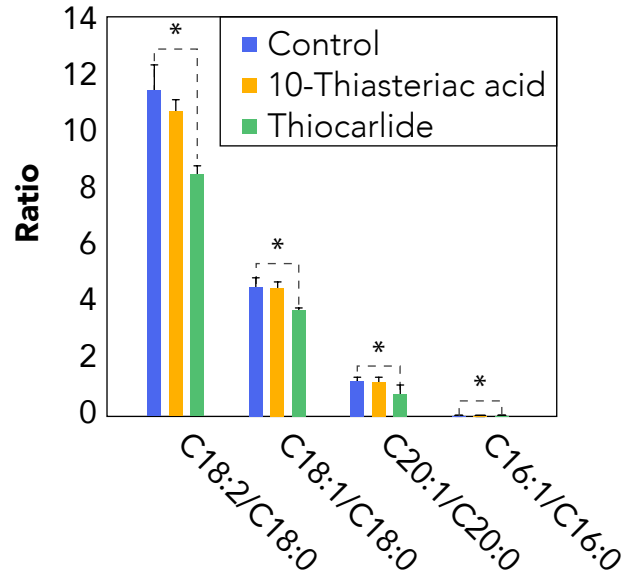


C

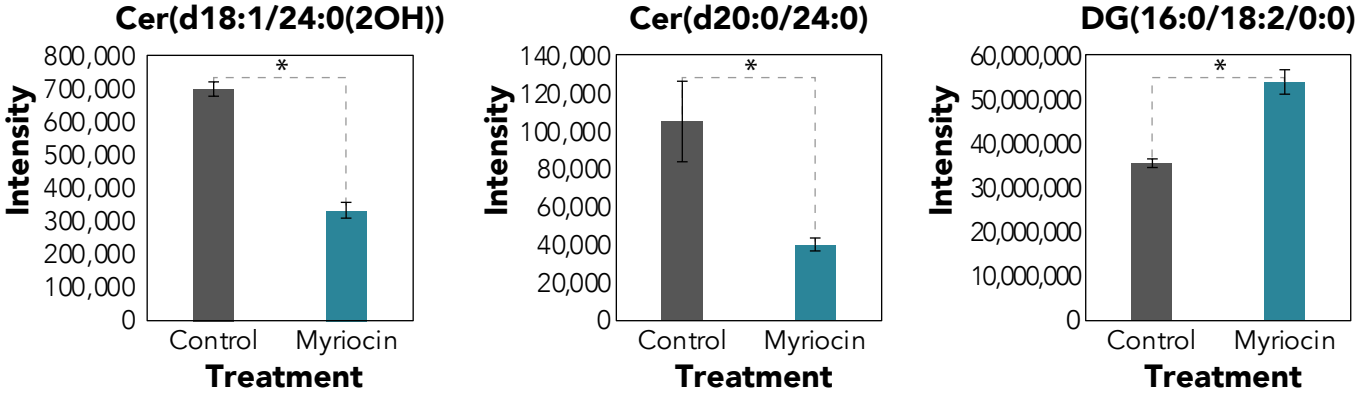


D

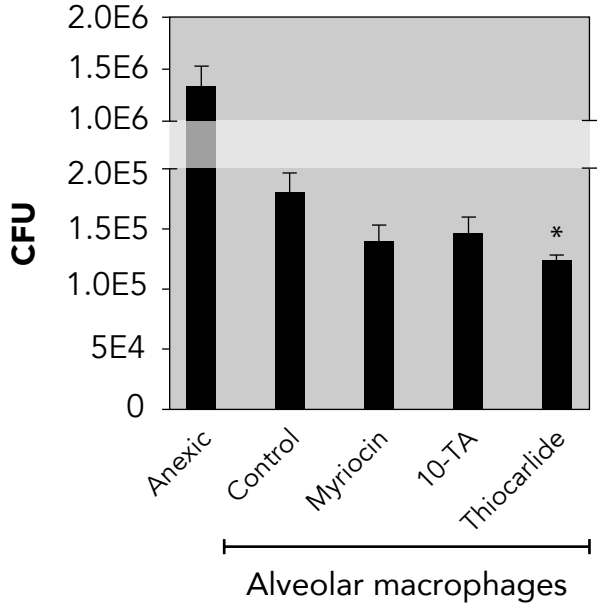


Figure 5

**Figure 5. Targeting sphingolipid and fatty acid desaturation pathways for drug development.**

(**A**) Minimum inhibitory concentration (MIC) of 10-thiastearic acid, thiocarlide and myriocin. The MICs were obtained from 5 independent experiments with 4 replicates each.

(**B**) Effect of fatty acid desaturase inhibitors in the fatty acid profile. Cells were grown in one half of each compound MIC and submitted to fatty acid analysis. The values represent the ratio of peak areas of unsaturated/saturate fatty acids.

(**C**) Effect of myriocin on the lipidomics profile. Cells were grown in one half of myriocin MIC and submitted to fatty acid analysis. The values represent the mass spectral signal intensity on the apex of the peak.

(**D**) Intracellular killing of *H. capsulatum* by alveolar macrophages treated with the inhibitors. Bars represent the combination of 4 independent experiments with 3 replicates each.

Statistical test: *$p \leq 0.05$ by Student *t*-test.

# Figure 6

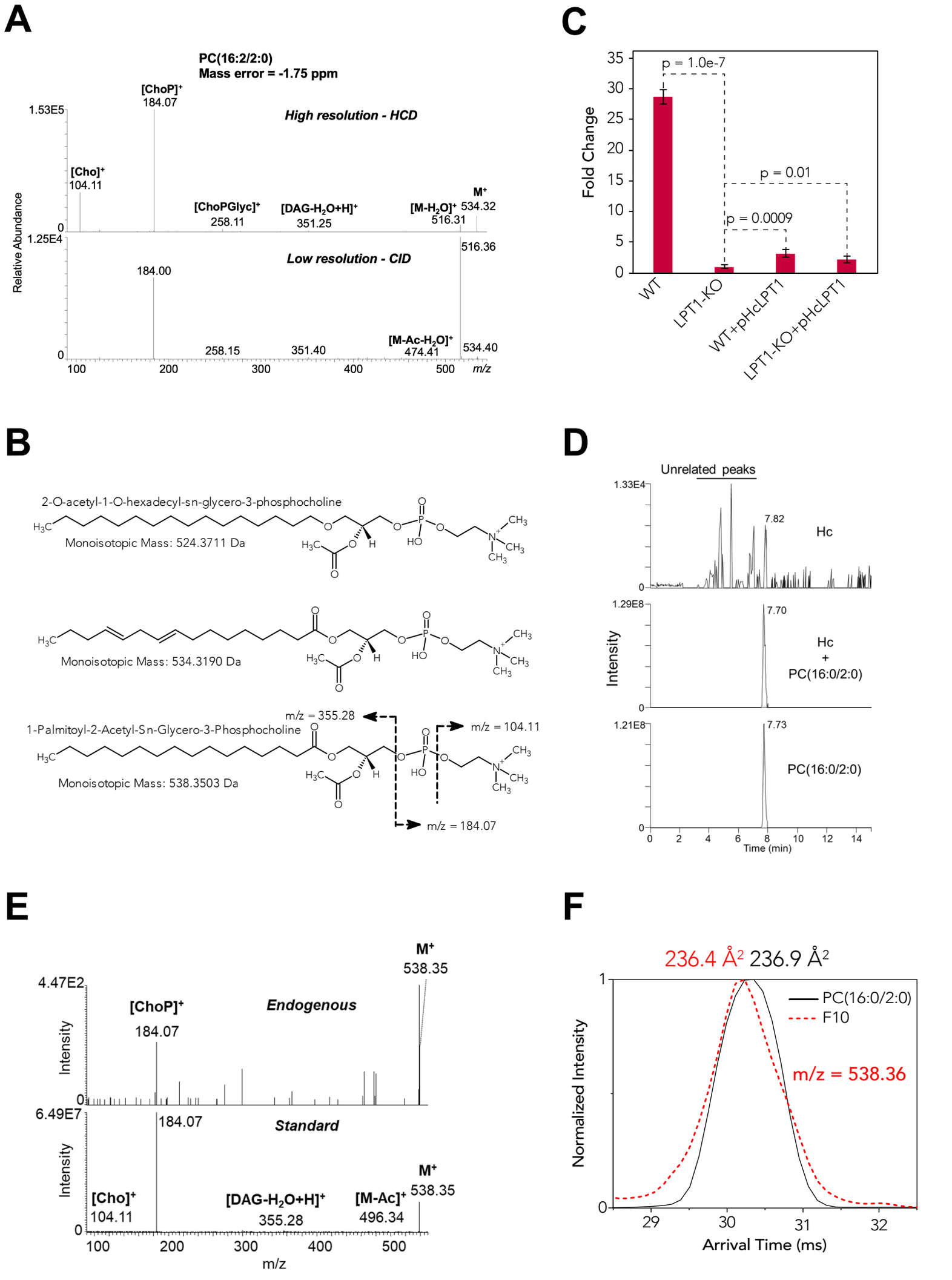
A
PC(16:2/2:0)
Mass error = -1.75 ppm
High resolution - HCD
[ChoP]+ 184.07
[Cho]+ 104.11
[ChoPGlyc]+ 258.11
[DAG-H2O+H]+ 351.25
[M-H2O]+ 516.31
M+ 534.32
Low resolution - CID
184.00
258.15
351.40
[M-Ac-H2O]+ 474.41
516.36
534.40
Relative Abundance
1.53E5
1.25E4
m/z
B
2-O-acetyl-1-O-hexadecyl-sn-glycero-3-phosphocholine
Monoisotopic Mass: 524.3711 Da
Monoisotopic Mass: 534.3190 Da
1-Palmitoyl-2-Acetyl-Sn-Glycero-3-Phosphocholine
Monoisotopic Mass: 538.3503 Da
m/z = 355.28
m/z = 104.11
m/z = 184.07
C
Fold Change
p = 1.0e-7
p = 0.01
p = 0.0009
WT
LPT1-KO
WT+pHcLPT1
LPT1-KO+pHcLPT1
D
Unrelated peaks
Hc
7.82
Hc + PC(16:0/2:0)
7.70
PC(16:0/2:0)
7.73
Intensity
Time (min)
E
Endogenous
[ChoP]+ 184.07
M+ 538.35
Standard
184.07
[Cho]+ 104.11
[DAG-H2O+H]+ 355.28
[M-Ac]+ 496.34
M+ 538.35
Intensity
m/z
F
236.4 Å2 236.9 Å2
PC(16:0/2:0)
F10
m/z = 538.36
Normalized Intensity
Arrival Time (ms)

**Figure 6. Identification and validation of platelet-activating factor (PAF) analogs in *Histoplasma capsulatum*.**

(**A**) Tandem-mass (MS/MS) spectra of the platelet-activating factor analog PC(16:2/2:0). The spectra show diagnostic fragments for phosphatidylcholine (Cho, ChoP and ChoPGlyc) and for an acetyl group (M-Ac-H2O).

(**B**) Structure, monoisotopic mass and tandem mass (MS/MS) fragments of PAF and analogs.

(**C**) Quantification of PC(16:1/2:0) in wild-type (WT) and *Lpt1*-knockout (KO) *Saccharomyces cerevisiae* strains transformed with a plasmid containing the *Histoplasma capsulatum Lpt1* gene (pHcLPT1). *S. cerevisiae* strains complemented or not with the pESC-URA plasmid with Hc-LPT1 gene under galactose-inducible promoter and grown in YNB medium supplemented with galactose. The experiment was performed with 4 replicates. Statistical test was done with student *t*-test considering equal distribution.

(**D**) LC-MS/MS analysis of *H. capsulatum* PC (16:0/2:0) against the synthetic standard. The graphs showed the same retention time of extracted ion chromatograms of *H. capsulatum* phospholipids, *H. capsulatum* phospholipids + standard and standard alone.

(**E-F**) MS/MS spectrum (**E**) and ion mobility-mass spectrometry (IMS-MS) (**F**) analyses of the PC (16:0/2:0) compared to the synthetic standard. The MS/MS analysis show the diagnostic fragment of phosphatidylcholines at *m/z* 184.07 (**F**), whereas the IMS-MS shows that the molecule has compatible arrival time and collision cross sections (stated in $Å^2$) with the standard.

Abbreviations: Ac, acetate; Cho, choline; ChoP, phosphocholine; ChoPGlyc; glycerophosphocholine; CID, collision-induced dissociation; DG, diacylglycerol; HCD, high-energy induced dissociation; M, mass; m/z, mass-over-charge ratio; ppm, parts-per-million.

**Figure 7**

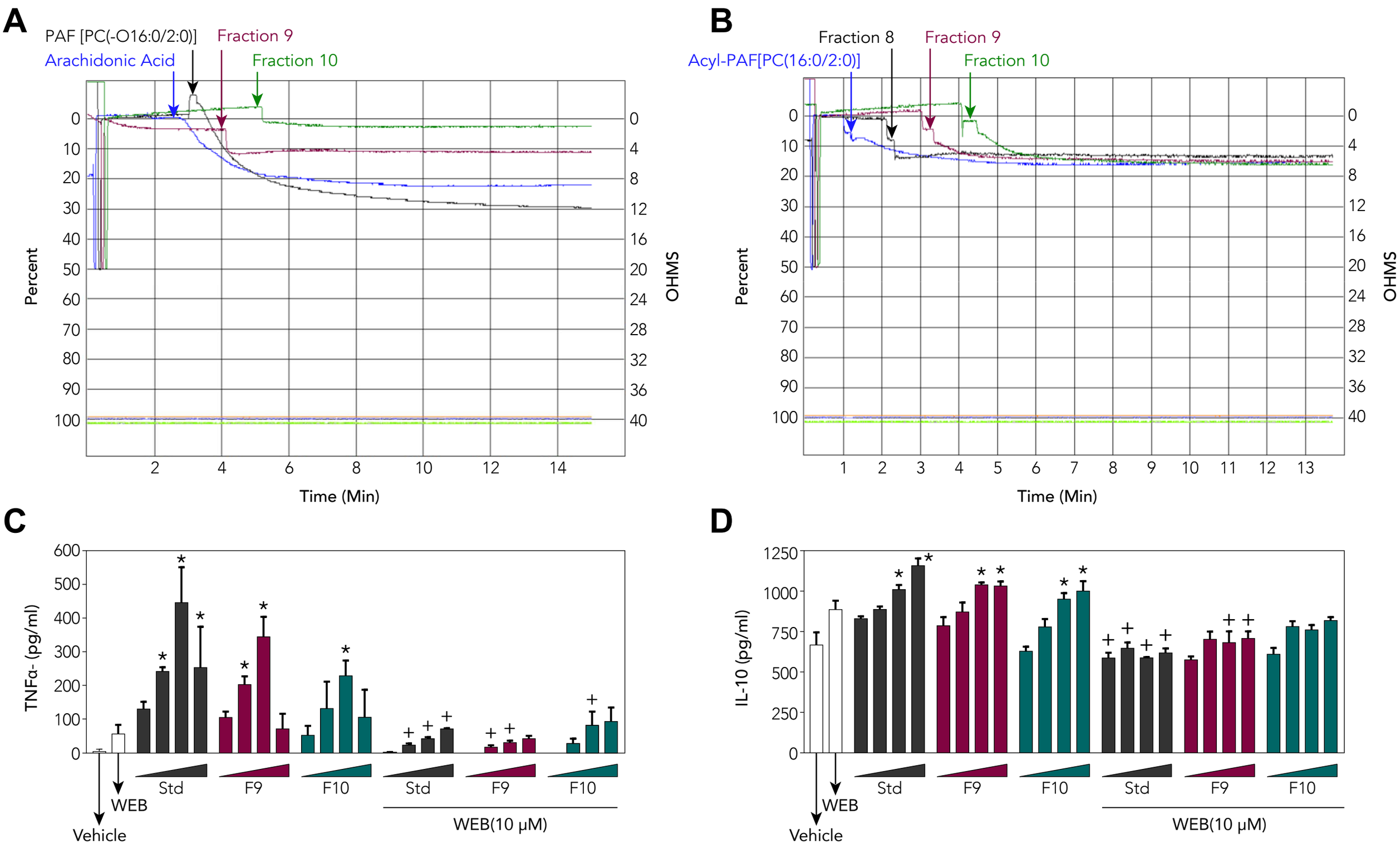
A
PAF [PC(-O16:0/2:0)]
Arachidonic Acid
Fraction 9
Fraction 10
Percent
OHMS
Time (Min)
B
Fraction 8
Fraction 9
Acyl-PAF[PC(16:0/2:0)]
Fraction 10
Percent
OHMS
Time (Min)
C
TNFα- (pg/ml)
Std
F9
F10
Std
F9
F10
WEB
Vehicle
WEB(10 μM)
D
IL-10 (pg/ml)
Std
F9
F10
Std
F9
F10
WEB
Vehicle
WEB(10 μM)

**Figure 7. Biological activity of *Histoplasma capsulatum* PAF analogs.**

(**A-B**) Platelet aggregation. Panels **A** and **B** are two measurements of platelet aggregation activity of HPLC fractions enriched with *H. capsulatum* PAF analogs (fractions 8-10). The arrows indicate the addition of each compound or HPLC fraction to samples of human peripheral blood and were measured by an aggregometer. The figure is representative of two independent experiments with similar results.

(**C-D**) Cytokine production. J774 macrophages were pre-treated or not with the PAF receptor antagonist (WEB2086 – 10 μM) for 30 minutes before the incubation with Std (acyl-PAF - PC (16:0/2:0)) and HPLC fractions enriched in *H. capsulatum* PAF analogs (fractions 9-10) for 24 hours. After the incubation, TNF-α (**C**) and IL-10 (**D**) were quantified by ELISA. The graphs show averages and SEM for 3 independent experiments. *$p < 0.05$ for comparisons against the solvent control (first bar). +$p < 0.05$ for respective groups in the presence and absence of WEB2086 by ANOVA followed by Tukey's multiple comparison test.

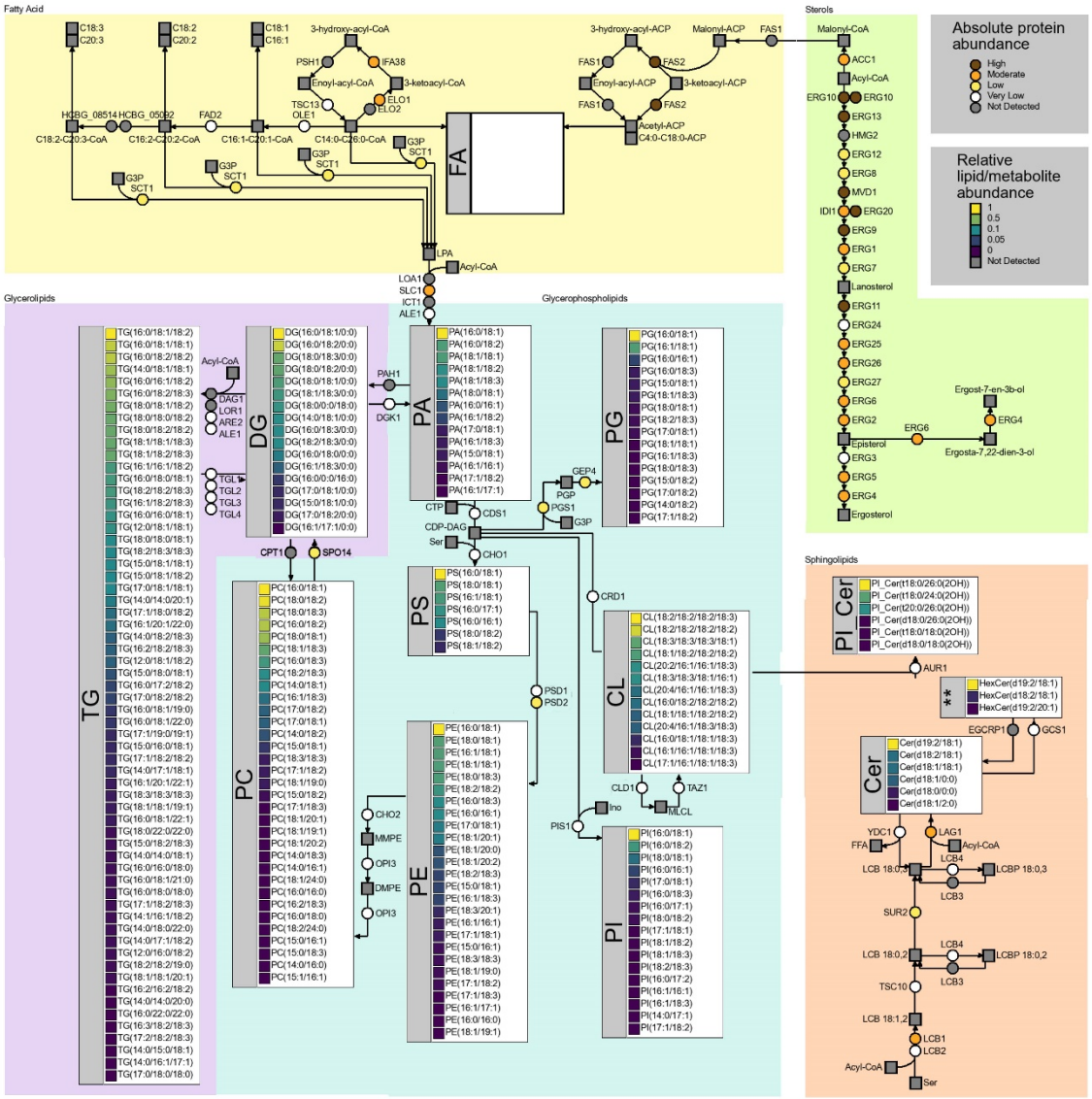


**Figure S1. Lipid metabolic pathway visualization tool.**
The lipid metabolic pathway built for *Histoplasma capsulatum* was converted into a lipidomics and proteomics data visualization tool using a script written in Perl and using the GD graphics package. The tool generates color-coded expression values based on the omics measurements.

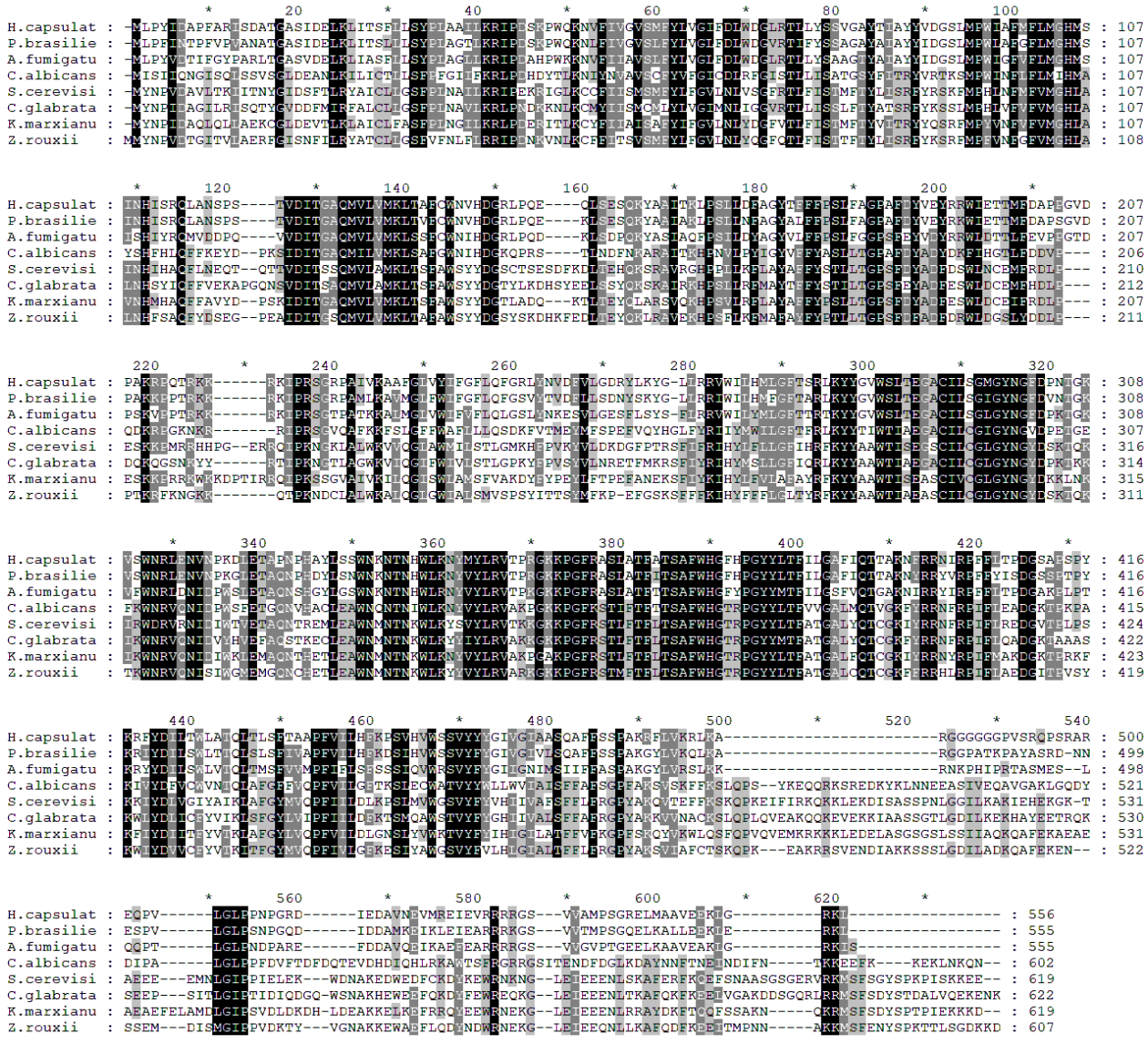


**Figure S2. Sequence alignment of *Histoplasma capsulatum* lysophosphatidylcholine acyltransferase LPT1 candidate gene and various homologs from other fungal species**.

*H. capsulatum* MBOAT family protein (NCBI accession number: EEH03012) was aligned with sequences from *Paracoccidioides brasiliensis* Pb18 (89% similarity, NCBI accession number: EEH50158), *Aspergillus fumigatus* Af293 (81% similarity, NCBI accession number: EAL85553), *Candida albicans* P37039 (56% similarity, NCBI accession number: KHC88112), *Saccharomyces cerevisiae* S288C (53% similarity, NCBI accession number: DAA10947), *Candida glabrata* (52% similarity, NCBI accession number: KTB01140), *Kluyveromyces marxianus* DMKU3-1042 (53% similarity, NCBI accession number: BAO40203) and *Zygosaccharomyces rouxii* (53% similarity, NCBI accession number: GAV49200).

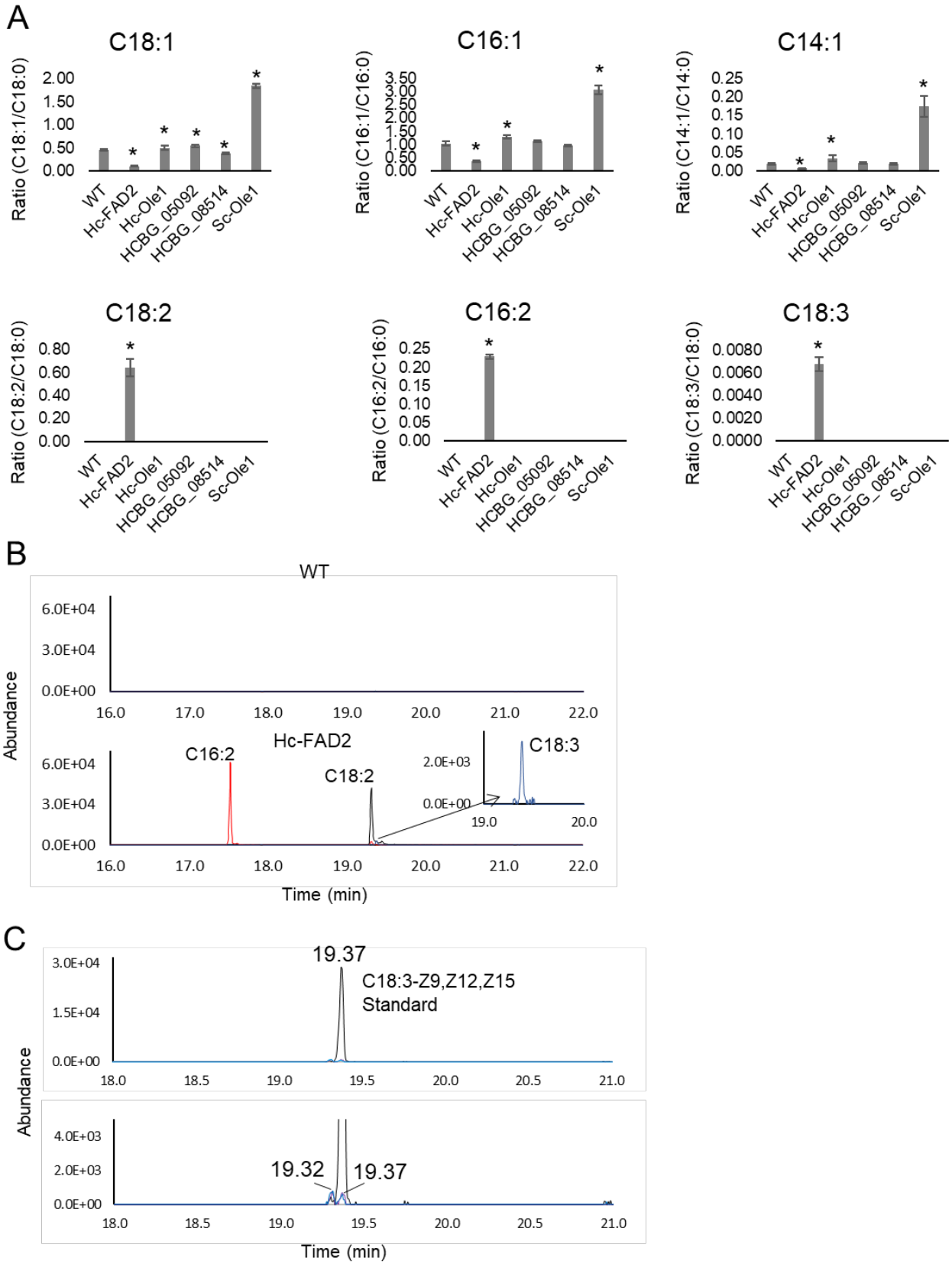
A
C18:1
Ratio (C18:1/C18:0)
2.00
1.50
1.00
0.50
0.00
C16:1
Ratio (C16:1/C16:0)
3.50
3.00
2.50
2.00
1.50
1.00
0.50
0.00
C14:1
Ratio (C14:1/C14:0)
0.25
0.20
0.15
0.10
0.05
0.00
C18:2
Ratio (C18:2/C18:0)
0.80
0.60
0.40
0.20
0.00
C16:2
Ratio (C16:2/C16:0)
0.25
0.20
0.15
0.10
0.05
0.00
C18:3
Ratio (C18:3/C18:0)
0.0080
0.0060
0.0040
0.0020
0.0000
WT
Hc-FAD2
Hc-Ole1
HCBG_05092
HCBG_08514
Sc-Ole1
B
WT
Hc-FAD2
Abundance
6.0E+04
3.0E+04
0.0E+00
16.0
17.0
18.0
19.0
20.0
21.0
22.0
C16:2
C18:2
C18:3
2.0E+03
0.0E+00
19.0
20.0
Time (min)
C
19.37
C18:3-Z9,Z12,Z15
Standard
3.0E+04
1.5E+04
0.0E+00
18.0
18.5
19.0
19.5
20.0
20.5
21.0
Abundance
4.0E+03
2.0E+03
0.0E+00
19.32
19.37
Time (min)

**Figure S3. Fatty acid composition analysis.**

(**A**) The analysis was done in *S. cerevisiae* strain transformed with the pESC-URA plasmid with *H. capsulatum* Ole1 (Hc-Ole1), FAD2 (Hc-FAD2), HCBG_08514 and HCBG_05092 genes and *S. cerevisiae* Ole1 (Sc-Ole1) gene under galactose-inducible promoter. Cells were grown in YNB medium and supplemented with galactose for 17 h. Lipids were extracted and hydrolyzed, and the resulting fatty acids were methylated and analyzed by gas chromatography-mass spectrometry. Levels of unsaturated fatty acids were expressed as ratios compared to their saturated counterpart. The experiment was performed in biological 4 replicates. Statistical test: *$p \leq 0.05$ compared to the control using Student *t*-test.

(**B**) Extracted ion chromatograms of fatty acids with 2 and 3 double bonds from control and *S. cerevisiae* strains expressing the *H. capsulatum* FAD2 gene. The chromatograms show that fatty acid species with 2 or 3 double bonds were not detected in wild-type *S. cerevisiae*.

(**C**) C18:3 fatty acids presence in *H. capsulatum* lipids. Lipids were extracted and hydrolyzed, and the resulting fatty acids were methylated and analyzed by gas chromatography-mass spectrometry. Comparison with external standards identified the peak at 19.37 minutes as α-linolenic acid, while the peak at 19.32 remained unidentified.

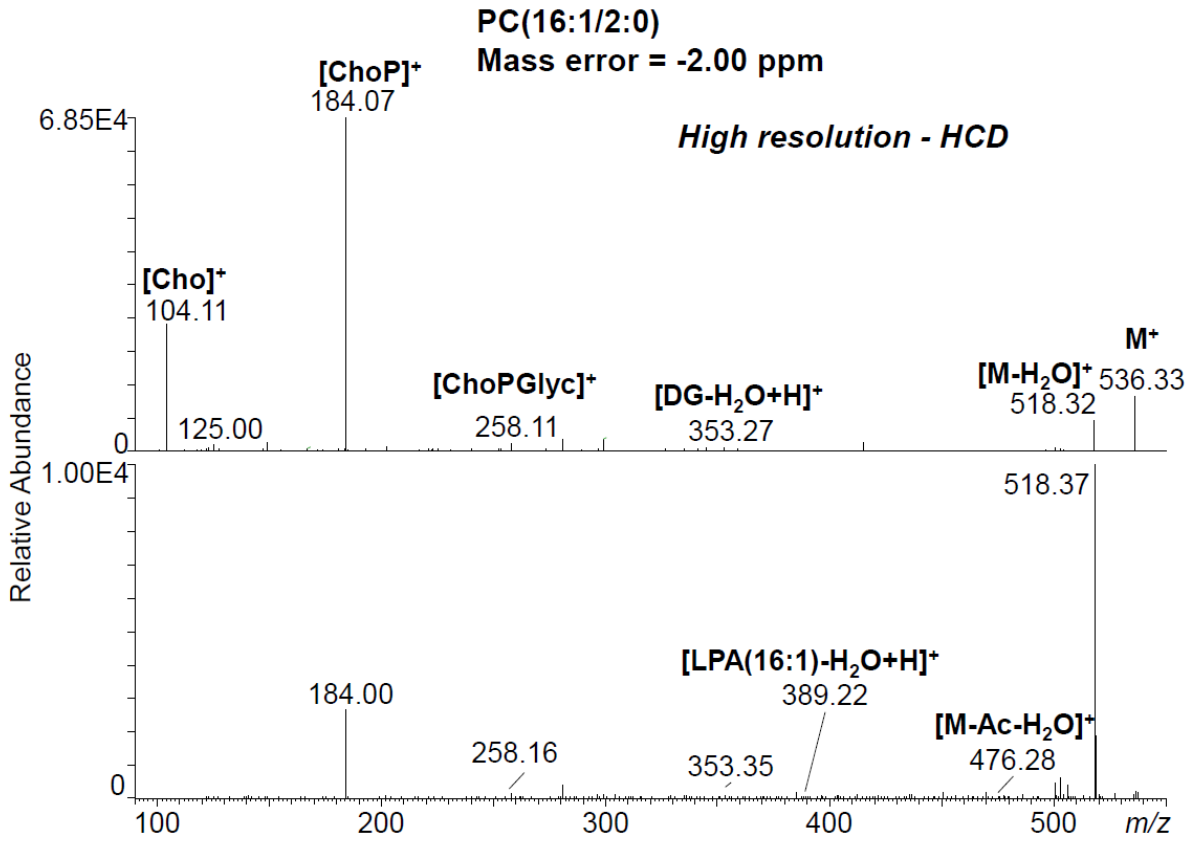


**Figure S4. Tandem-mass (MS/MS) spectra of the platelet-activating factor analog PC(16:1/2:0).**

Abbreviations: Ac, acetate; Cho, choline; ChoP, phosphocholine; ChoPGlyc; glycerophosphocholine; CID, collision-induced dissociation; DG, diacylglycerol; HCD, high-energy induced dissociation; M, mass; m/z, mass-over-charge ratio; ppm, parts-per-million. The spectra show diagnostic fragments for phosphatidylcholine (Cho, ChoP and ChoPGlyc) and for an acetyl group (M-Ac-$H_2O$).